MIF-mediated crosstalk between THRSP^{+} hepatocytes and CD74^{+} lipid-associated macrophages in hepatic peri-portal zone drives MASH

VISUAL ABSTRACT

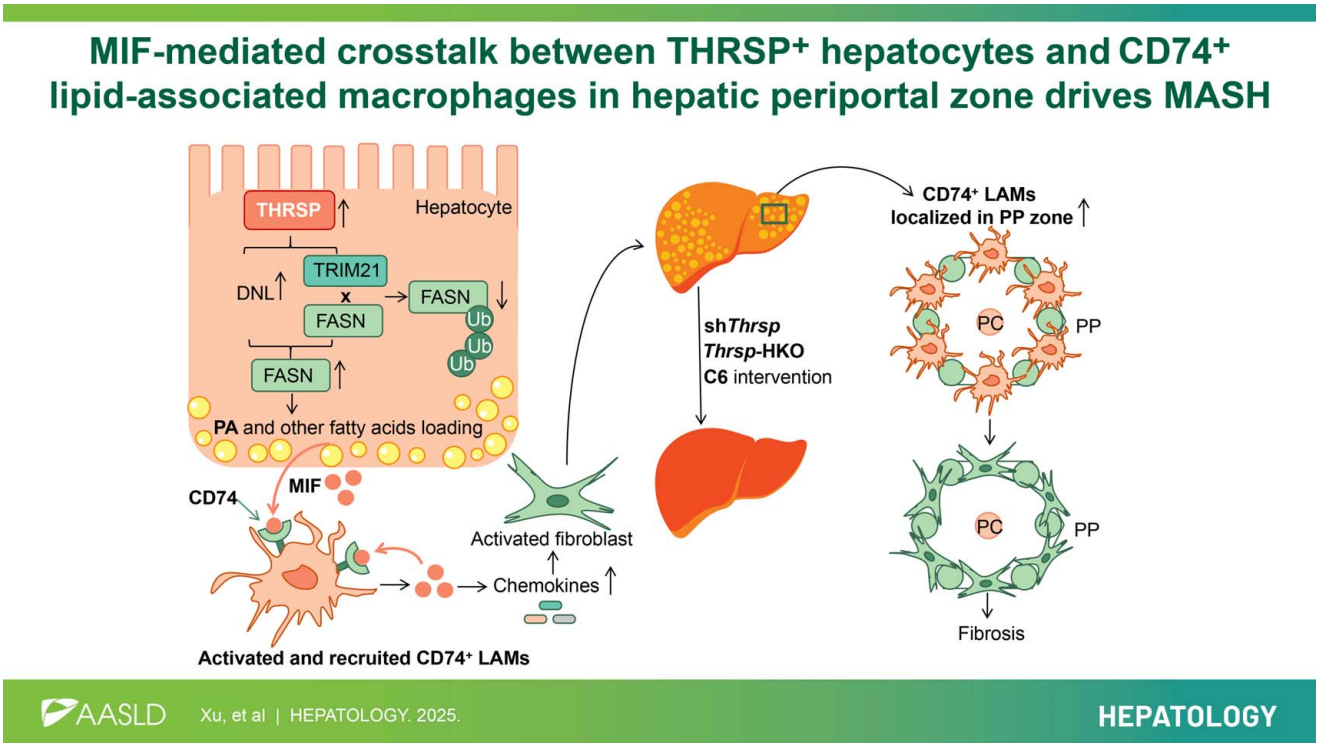

Received: 26 November 2024 | Accepted: 21 May 2025

DOI: 10.1097/HEP.0000000000001429

ORIGINAL ARTICLE

OPEN

MIF-mediated crosstalk between THRSP+ hepatocytes and CD74+ lipid-associated macrophages in hepatic periportal zone drives MASH

Xu Xu[1,2] | Huagen Li[3] | Hai Lin[4] | Qichao Li[5,6] | Yuenan Liu[1] | Weijun Huang[1] | Jundong Yang[1] | Niannian Li[1] | Zhenfei Gao[1] | Shengming Wang[1] | Hangdong Shen[1] | Wenjun Xue[1] | Haolin Yuan[1] | Wei Wang[7] | Jianwei Shuai[6] | Junli Liu[2] | Shankai Yin[1] | Feng Liu[1]

[1]Department of Otolaryngology Head and Neck Surgery, Otolaryngological Institute of Shanghai Jiao Tong University, Shanghai Sixth People's Hospital Affiliated to Shanghai Jiao Tong University School of Medicine, Shanghai, China

[2]Department of Endocrinology and Metabolism, Shanghai Diabetes Institute, Shanghai Sixth People's Hospital Affiliated to Shanghai Jiao Tong University School of Medicine, Shanghai, China

[3]Department of General Surgery, Beijing Friendship Hospital, Capital Medical University, Beijing, China

[4]Wenzhou Key Laboratory of Biophysics, Wenzhou Institute, University of Chinese Academy of Sciences, Wenzhou, Zhejiang, China

[5]Postgraduate Training Base Alliance, Wenzhou Medical University, Wenzhou, Zhejiang, China

[6]Oujiang Laboratory (Zhejiang Laboratory for Regenerative Medicine, Vision and Brain Health), Wenzhou Institute, University of Chinese Academy of Sciences, Wenzhou, Zhejiang, China

[7]Department of General Surgery, Shanghai Sixth People's Hospital Affiliated to Shanghai Jiao Tong University School of Medicine, Shanghai, China

Correspondence
Jianwei Shuai, Wenzhou Institute, University of Chinese Academy of Sciences, Wenzhou, Zhejiang 325001, China; Oujiang Laboratory (Zhejiang Lab for Regenerative Medicine, Vision and Brain Health), Wenzhou, Zhejiang 325001, China.
Email: shuaijw@wiucas.ac.cn

Junli Liu, Department of Endocrinology and Metabolism, Shanghai Diabetes Institute, Shanghai Sixth People's Hospital Affiliated to Shanghai Jiao Tong University School of Medicine, Shanghai 200233, China.
Email: liujunli@sjtu.edu.cn

Abstract

Background and Aims: Spatial location of steatosis is closely related to the progression of metabolic dysfunction–associated steatohepatitis (MASH), and reports suggest lipid-associated macrophages (LAMs) facilitate this progression. However, the underlying mechanisms remain elusive.

Approach and Results: Spatial transcriptomics (ST) data revealed a significant increase in myeloid cells and MASH-related genes in the hepatic periportal (PP) zone of MASH mice, suggesting a vital role of the PP zone in MASH progression. THRSP (SPOT14), involved in fatty acid synthesis, was

Abbreviations: CETSA, cellular thermal shift assay; Co-IP, co-immunoprecipitation; CQ, chloroquine; DAMP, danger-associated molecular pattern; DNL, de novo lipogenesis; FASN, fatty acid synthase; FFA, free fatty acid; GC–MS, gas chromatography–mass spectrometry; GEO, Gene Expression Omnibus; GTT, glucose tolerance test; IHC, immunohistochemistry; ITT, insulin tolerance test; LAMs, lipid-associated macrophages; LCFAa, long-chain fatty acids; MAFL, metabolic dysfunction–associated fatty liver; MASH, metabolic dysfunction–associated steatohepatitis; MASLD, metabolic dysfunction–associated fatty liver disease; MDM, monocyte-derived macrophage; MIF, macrophage migration inhibitory factor; mIHC, multiplex IHC; ORO, Oil Red O; PA, palmitic acid; PC, pericentral; PP, periportal; QuSAGE, quantitative set analysis for gene expression; Res, Resmetirom; SFFA, saturated FFA; SREBP-1c, sterol regulatory element-binding protein 1c; ST, spatial transcriptomics; TBG, thyroxine-binding globulin; TC, total cholesterol; TG, triglycerides; THRSP, thyroid hormone-responsive protein; USFFA, unsaturated FFA; WB, western blot; WD, western diet.

Xu Xu, Huagen Li, and Hai Lin contributed equally to this work.

Clinical trial number: ChiCTR2400086795.

Supplemental Digital Content is available for this article. Direct URL citations are provided in the HTML and PDF versions of this article on the journal's website, www.hepjournal.com.

Shankai Yin, Department of Otolaryngology Head and Neck Surgery, Otolaryngological Institute of Shanghai Jiao Tong University, Shanghai Sixth People's Hospital Affiliated to Shanghai Jiao Tong University School of Medicine, Shanghai 200233, China.
Email: skyin@sjtu.edu.cn

Feng Liu, Department of Otolaryngology Head and Neck Surgery, Otolaryngological Institute of Shanghai Jiao Tong University, Shanghai Sixth People's Hospital Affiliated to Shanghai Jiao Tong University School of Medicine, Shanghai 200233, China.
Email: liufeng@sibs.ac.cn

markedly elevated in the livers of MASH patients and mice. Notably, CellPhoneDB analysis identified strong interactions between CD74 and macrophage migration inhibitory factor (MIF) within the *Thrsp*-high zone. Furthermore, *Thrsp*, *Cd74*, *Mif*, *Col3a1*, and LAMs markers were prominently colocalized in the hepatic PP zone of MASH mice, suggesting that *Thrsp*-mediated crosstalk in this region played a crucial role in MASH progression. *Thrsp* overexpression/knockout experiments confirmed that THRSP drove MASH progression by recruiting $CD74^+$ LAMs mediated by MIF. Mechanistically, THRSP promoted hepatic palmitic acid (PA) synthesis, mainly by promoting hepatic de novo lipogenesis, and disturbing the binding of FASN–TRIM21, thereby inhibiting FASN ubiquitination. $CD74^+$ LAMs were activated and recruited by chemokine-like MIF secreted from hepatocytes and macrophages stimulated with PA. Additionally, the compound C6, identified as a *THRSP* inhibitor, significantly ameliorated MASH in mice.

Conclusions: Our study demonstrates that THRSP drives MASH progression by recruiting $CD74^+$ LAMs mediated by MIF in the hepatic PP zone, providing novel insights into the spatial zonation and crosstalk between lipogenic hepatocytes and LAMs that may result in novel therapies for MASH.

Keywords: fatty acid synthase, inflammation, liver microenvironment, palmitic acid, spatial zonation

INTRODUCTION

Metabolic dysfunction–associated steatotic liver disease (MASLD) is the hepatic manifestation of metabolic syndrome and is currently the most prevalent liver disease worldwide.[1–3] MASLD encompasses a histological spectrum ranging from non-progressive hepatic steatosis [metabolic dysfunction–associated fatty liver (MAFL)] to progressive steatohepatitis [metabolic dysfunction–associated steatohepatitis (MASH)]. The progressive form is associated with steatosis, ballooned hepatocytes, lobular inflammation, and fibrosis. Unlike MAFL, MASH significantly heightens the risk of liver-related mortality and cardiovascular events.[4,5] Despite the severe adverse outcomes of MASH, there is only one FDA-approved drug, Resmetirom (Res), an oral thyroid hormone receptor agonist.[6] Addressing the progression from MAFL to MASH is critical, yet the underlying pathological mechanisms remain incompletely understood.

Liver is a highly heterogeneous organ composed of hexagonal lobules, with zonation effects impacting cell type, distribution, and function along nutrient, oxygen, and hormone gradients that develop as blood flows from the periportal (PP) zone, where the portal vein, hepatic artery, and bile ducts are located, toward the pericentral (PC) zone at the center of the lobule. This non-uniform distribution, termed "liver zonation," underlies hepatic functions. Liver zonation plays a fundamental role in both normal liver physiology and the pathogenesis of fatty liver diseases.[7] Fatty acids serve as the most energy-dense form of storage and are synthesized from excess glucose during high-fat, high-carbohydrate intake, a process known as de novo lipogenesis (DNL).[8] DNL process was closely linked to AKT/mTOR signaling, and AKT activation induced expressions of lipogenic genes such as fatty acid synthase (FASN), a key enzyme in DNL.[9,10] While elevated free fatty acids (FFA) levels are implicated in the onset and progression of MASLD.[11] Notably, palmitic acid (PA, C16:0) and other saturated FFA (SFFA) exhibit more severe lipotoxicity than unsaturated FFA (USFFA), as they induce hepatocyte lipoapoptosis,[12–14] leading to the release of danger-associated molecular patterns (DAMPs) which can induce liver inflammation, fibrosis, and cirrhosis, primary features of MASH.[15,16] During liver injury, monocytes extensively infiltrate the liver and differentiate into proinflammatory monocyte-derived macrophages, and replace resident KCs as the primary macrophage population.[17] Intrahepatic crosstalk plays a vital role in tissue homeostasis and injury response.[18]

These findings suggest that PA-induced DAMPs, mediated by KCs and monocytes, are a key promoter of MASH progression. The zonated dynamics of intrahepatic FFA and their role in MAFL-to-MASH progression remain poorly understood.

Hepatic TREM2$^+$ lipid-associated macrophages (LAMs), marked by *Gpnmb*, *Cd9*, *Spp1*, and *Ms4a7* expression, form crown-like structures that drive MASH progression.[18–21] Macrophage migration inhibitory factor (MIF) plays a critical role in inflammatory diseases. PA dose-dependently stimulated MIF secretion in MIN6 cells.[22] In the liver, MIF is secreted by both hepatocytes and monocytes/macrophages.[23] MIF signals via CD74 receptor and coreceptors CXCR2, CXCR4, which are expressed on KCs and circulating monocytes, allowing MIF to activate KCs and recruit peripheral monocytes.[24] Hepatocyte MIF, as a multifunctional cytokine/chemokine, has been proven to coordinately regulate chemokine expression in alcohol-associated hepatitis.[25] Thyroid hormone-responsive protein (THRSP), a modulator of fatty acid synthesis, is highly expressed in lipogenic tissues, such as the liver.[26,27] While THRSP (expressed in hepatocyte nuclei/cytoplasm; Liver Cell Atlas) is known to regulate lipogenesis via transcriptional pathways,[28–30] its potential non-transcriptional mechanisms and precise role in MASH progression remain undefined.

Our data reveal that THRSP drives MASH progression by recruiting CD74$^+$ LAMs mediated by chemokine-like MIF in the hepatic PP zone, leading to inflammation and advanced fibrosis. We identify a novel THRSP-inhibiting compound with therapeutic potential for MASH. These findings position THRSP as a therapeutic target for MASH, with PP zone-specific crosstalk between lipogenic hepatocytes and LAMs driving disease progression—a paradigm enabling precision intervention strategies.

METHODS

Animal studies

Eight-week-old male C57BL/6J mice (Beijing Vital River Laboratory Animal Technology Co., Ltd.) were kept under a 12-hour light/dark cycle and had ad libitum access to standard chow diet with normal water or modified western diet (WD) containing 40% kcal from fat and 0.2% cholesterol (modified WD, D221202, Dyets) along with a high fructose–glucose solution (23.1 g/L D-fructose +18.9 g/L D-glucose) for 8 weeks (MAFL model) and 16 weeks (MASH model).[31–33] From the 13th week of feeding, subsets received daily oral Res (10 mg/kg) and intraperitoneal (i.p.) compound C6 (10 or 30 mg/kg) for 4 weeks. Animal protocols were approved by the Animal Care and Use Committee at the University of Shanghai Jiao Tong University and strictly conducted in accordance with the ARRIVE (Animals in Research: Reporting In Vivo Experiments) statement. The study received approval from the Ethics Committee of Shanghai Sixth People's Hospital (Approval No. 2023-0020).

To establish *Thrsp* overexpression and knockdown mice, AAV8-NC, AAV8-*Thrsp*, AAV8-shNC, and AAV8-sh*Thrsp* were administered via i.v. injection (1×10^{12} vector genomes/mouse) into C57BL/6J mice. After 3 weeks of AAV injection, mice were fed with a custom WD, including a modified WD accompanied by high fructose–glucose solution (custom WD) for 16 weeks. The AAV8 vectors used in this study were constructed with the thyroxine-binding globulin (TBG) promoter, which was liver-specific. Primers for *Thrsp* overexpression and knockdown mice construction were listed in Supplemental Tables S1, S2, http://links.lww.com/HEP/J840.

Thrsp-flox mice were purchased from GemPharmatech (T019707). The homozygous *Thrsp*-flox/flox mice received tail vein injections of either AAV8-TBG-SfGFP (control) or AAV8-TBG-NLS-Cre (1×10^{12} vector genomes/mouse; OBiO Technology) to generate *Thrsp*-HKO mice. All mice were fed a custom WD for 16 weeks, after 12 weeks of feeding, subsets received C6 (30 mg/kg/d) for 4 weeks.

Human liver samples

Human liver tissue samples were obtained from patients who had undergone liver resections at the Department of General Surgery, Shanghai Sixth People's Hospital, China. Participants were without alcohol consumption (>20 g/d in women and >30 g/d in men), active infectious disease, pregnancy, or any contraindication for liver resection. All patients provided written informed consent. The study protocol was approved by the Ethics Committee of Shanghai Sixth People's Hospital, Approval No. 2024-KY-070 (K), before study commencement.

Public dataset collection and analysis

Single-cell/single-nucleus RNA sequencing (sc/snRNA-seq) data from human and murine liver tissues were collected and analyzed for cell typing of spatial transcriptomic (ST) data. GSE192742 was downloaded from the Gene Expression Omnibus (GEO) database.[34]

Spatial transcriptomics

Fresh liver samples (MAFL/MASH) were OCT-embedded, snap-frozen, and analyzed by 10x Visium spatial transcriptomics per manufacturer's protocol,[35,36] with cell typing via cell2location[37] (see Supplemental Methods for details http://links.lww.com/HEP/J840).

Quantitative set analysis for gene expression analysis

Quantitative set analysis for gene expression (QuSAGE) was used to analyze the enrichment of specified gene sets related to MASH[38] and other metabolism-related gene sets (KEGG database) in the livers from the MAFL and MASH groups. Additional details are found in the Supplemental Information, http://links.lww.com/HEP/J840.

CellPhone analysis

We used CellPhoneDB (V1.1.0) to perform cell communication analysis in the high *Thrsp*-expressing clusters (clusters 0 and 7) in the liver of the MASH mice. The results of the top 15 communication pairs based on *p* values were presented.[39] Additional details are found in the Supplemental Information http://links.lww.com/HEP/J840.

Co-immunoprecipitation assay

Co-immunoprecipitation (Co-IP) assays were performed to validate the protein interactions. Protein lysates were incubated overnight at 4°C with the indicated antibodies (Supplemental Table S3, http://links.lww.com/HEP/J840), followed by 4 hours of rotation with Dynabeads Protein A/G (10002D/10003D, Invitrogen) at 4°C. The immunoprecipitated complexes were then eluted in SDS buffer and analyzed by immunoblotting. Primers for *Thrsp* overexpression plasmid construction are listed in Supplemental Table S4, http://links.lww.com/HEP/J840.

Single-nucleus RNA-seq and analysis

Single liver nuclei were isolated from AAV8-NC and AAV8-*Thrsp*–treated MASH mice and then processed using the 10x Genomics Chromium Next GEM Single Cell 3' Kit v3.1 (1000268) according to the manufacturer's protocol. Libraries were constructed and sequenced by OE Biotech. Additional details are found in the Supplemental Information, http://links.lww.com/HEP/J840.

Cell isolation and flow cytometry

Liver-derived single cells were obtained by collagenase IV/DNase I digestion (1 mg/mL, 200 U/mL; 37°C, 30 min), stained with fluorescent antibodies (CD45-PE, CD11b-PE-Cy7, Ly6C-FITC, CD74-AF647, BODIPY FL C16; 30 min, 4°C), and analyzed by flow cytometry (BD Symphony A5, FlowJo v10). Additional details are found in the Supplemental Information, http://links.lww.com/HEP/J840.

IP coupled with mass spectrometry (IP/MS)

Proteins were extracted from *Thrsp*-transfected AML12 cells, and IP was performed using THRSP antibody (2 μg, Proteintech) against protein A beads (1:10 volume, Invitrogen). The isolated immunoprecipitates were analyzed using MS performed by PTM BIO.

MIF content assay

The MIF levels in the supernatant of AML12 cells, in which *Thrsp* was either overexpressed or knocked down, were measured after 24 hours of stimulation with or without PA (0.5 mM). Subsequently, half of the supernatant from the aforementioned AML12 cells was mixed with an equal volume of fresh medium to culture RAW264.7 cells for an additional 24 hours, followed by assessment of MIF levels in the RAW264.7 cell supernatant. MIF content was detected by using the Mouse MIF ELISA Kit (Proteintech, KE10027).

Cellular thermal shift assay

Cellular thermal shift assay (CETSA) was performed to assess compound-target engagement. Cell extracts from *Thrsp*-transfected AML12 cells were incubated with C6 (10 μM) or DMSO (10 min, 23°C), aliquoted (60 μL), and heated at graded temperatures (3 min). After centrifugation (100,000*g*, 20 min, 4°C), supernatants were analyzed by Western blot.[40]

FFA assay

The fresh liver tissues were harvested from mice, and the contents of medium-chain and long-chain FFA were analyzed by gas chromatography–mass spectrometry (GC–MS) performed by BioNovoGene.

WB, quantitative real-time reverse transcription PCR, and immunofluorescence

The procedures of WB and quantitative real-time reverse transcription PCR (RT-PCR) were performed as previously described.[41] Proteins were separated by 4%–12% sodium dodecyl sulfate–polyacrylamide gel electrophoresis. Total RNA isolation kit, the PrimeScript RT reagent used for cDNA synthesis, and SYBR Green PCR kits (Vazyme) were used to perform RT-PCR. Additional details are found in the Supplemental Information, http://links.lww.com/HEP/J840.

Liver tissues were processed for immunofluorescence (IF) staining as previously described.[42] The antibodies

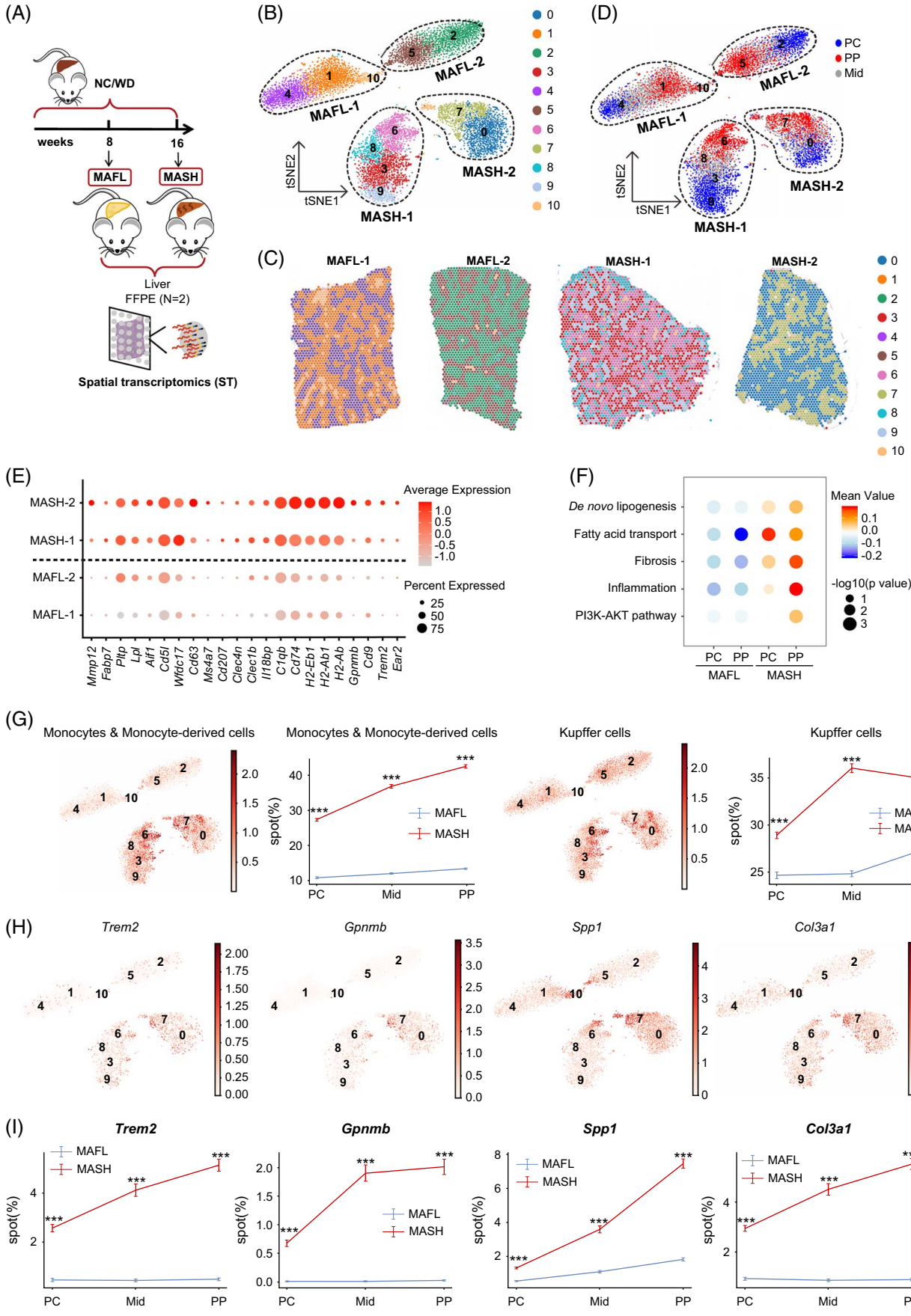
(A)
NC/WD
weeks
8
16
MAFL
MASH
Liver
FFPE (N=2)
Spatial transcriptomics (ST)
(B)
MAFL-1
MAFL-2
MASH-1
MASH-2
tSNE1
tSNE2
(D)
PC
PP
Mid
(C)
(E)
Average Expression
Percent Expressed
Mmp12
Fabp7
Pltp
Lpl
Aif1
Cd5l
Wfdc17
Cd63
Ms4a7
Cd207
Clec4n
Clec1b
Il18bp
C1qb
Cd74
H2-Eb1
H2-Ab1
H2-Ab
Gpnmb
Cd9
Trem2
Ear2
(F)
De novo lipogenesis
Fatty acid transport
Fibrosis
Inflammation
PI3K-AKT pathway
Mean Value
-log10(p value)
PC PP PC PP
MAFL
MASH
(G)
Monocytes & Monocyte-derived cells
Kupffer cells
spot(%)
MAFL
MASH
PC
Mid
PP
(H)
Trem2
Gpnmb
Spp1
Col3a1
(I)
Trem2
Gpnmb
Spp1
Col3a1

FIGURE 1 The spatial zonation characteristics in the livers of MAFL and MASH mice. (A) The experimental diagram of ST. NC: normal chow, WD: custom western diet, including modified western diet containing 40% kcal from fat and 0.2% cholesterol, accompanied by high fructose–glucose solution (23.1 g/L D-fructose +18.9 g/L D-glucose). (B) The cell clustering (clusters 0–10) of livers from MAFL and MASH mice is shown in the tSNE. (C) The spatial distribution of cell clustering (clusters 0–10) in the liver sections from MAFL and MASH mice. N = 2/group, mice. (D) Zonation pattern of lobule PC and PP as the marker genes (PC: *Oat*, blue; PP: *Sds*, red) indicated. (E) The bubble plot of differential expression genes in the livers between the MAFL and MASH groups. The depth of color represents the average expression of the gene, and the size of the spot represents the percentage of the gene expression. (F) The bubble plot of gene sets enrichment analysis in the PC and PP zone of livers from MAFL and MASH mice. (G) The tSNE and line chart showing expressions and distributions of monocytes, monocyte-derived cells, and KCs in the livers from MAFL and MASH mice. (H, I) The expressions and distributions of *Trem2*, *Gpnmb*, *Spp1*, and *Col3a1* in livers from both groups (n = 2/group, mice). Mid, middle region. *p* Values were calculated by 2-way ANOVA followed by Tukey multiple comparison test (F, H). ***$p < 0.001$. Abbreviations: MAFL, metabolic dysfunction–associated fatty liver; MASH, metabolic dysfunction–associated steatohepatitis. PC, pericentral; PP, periportal; ST, spatial transcriptomics

for WB, IF, and primers used in this assay were listed in Supplemental Table 3 (information about antibodies used in WB and IF), http://links.lww.com/HEP/J840, Supplemental Table 5 (primers for qPCR), http://links.lww.com/HEP/J840. The raw/unprocessed images were provided in Supplemental Digital Content Original images, http://links.lww.com/HEP/K229.

Oil Red O (ORO) staining in primary hepatocytes

Primary hepatocytes were transfected with NC/*Thrsp* and si-NC/si-*Thrsp* for 48 hours and then treated with bovine serum albumin or a palmitic acid (PA, 0.5 mM) and oleic acid (OA, 1 mM) mixture (PAOA) for 12 hours. Subsequently, they were stained using the ORO stain kit by the manufacturer's protocols (Sangon Biotech).[43,44] The primers for *Thrsp* overexpression plasmid construction and siRNA target sequences for *Thrsp* knockdown were listed in Supplemental Tables S4, http://links.lww.com/HEP/J840, and S6, http://links.lww.com/HEP/J840.

Histological analysis

Paraffin-embedded liver tissues were subjected to H&E, Sirius Red staining, and immunohistochemistry (IHC) and tyramide signal amplification multiplex IHC (mIHC) analyses. Frozen liver sections were used for ORO staining to visualize lipid droplets. Additional details are found in the Supplemental Information, http://links.lww.com/HEP/J840.

Glucose tolerance test (GTT) and insulin tolerance test (ITT)

Approximately 16 hours of overnight fasting before mice were injected i.p. with glucose (2 g/kg) for GTT measurement, and mice were fasted for 6 hours before being injected i.p. with regular human insulin (0.75 U/kg) for insulin resistance measurement. Additional details are found in the Supplemental Information, http://links.lww.com/HEP/J840.

Biochemical measurement

The total triglycerides (TG) and total cholesterol (TC) in liver tissues, AST, ALT, and creatinine levels in serum were determined using commercial kits by the manufacturer's protocols (Nanjing Jiancheng Bioengineering Institute).

Statistical analysis

Data were presented as mean ± SE. Unpaired 2-tailed *t* tests were used for comparison of the 2 groups. Statistical comparisons were made by one-way ANOVA, followed by Tukey post hoc tests or 2-way ANOVA, followed by Sidak/Tukey multiple comparison test with between-group differences for at least 3 groups' comparisons. Significance was defined as $p < 0.05$.

RESULTS

Zonation characteristics in the livers of MAFL and MASH mice

To investigate the potential mechanisms of driving the progression from MAFL to MASH, we employed custom WD-fed mouse models replicating the human MAFL/MASH disease conditions. Our data demonstrated a significant increase in hepatic FFA as the progression from MAFL to MASH (Supplemental Figure S1, http://links.lww.com/HEP/J840). Fresh liver tissues from both disease stages were analyzed using 10x Visium spatial transcriptomics (Figure 1A), and publicly available single-nucleus RNA sequencing data from WD-fed mice (GSE192742) were integrated using the cell2location method. *t*-SNE analysis identified 11 hepatic clusters (5 MAFL, 6 MASH) with disease-state-specific groupings (Figures 1B, C). Enrichment analysis

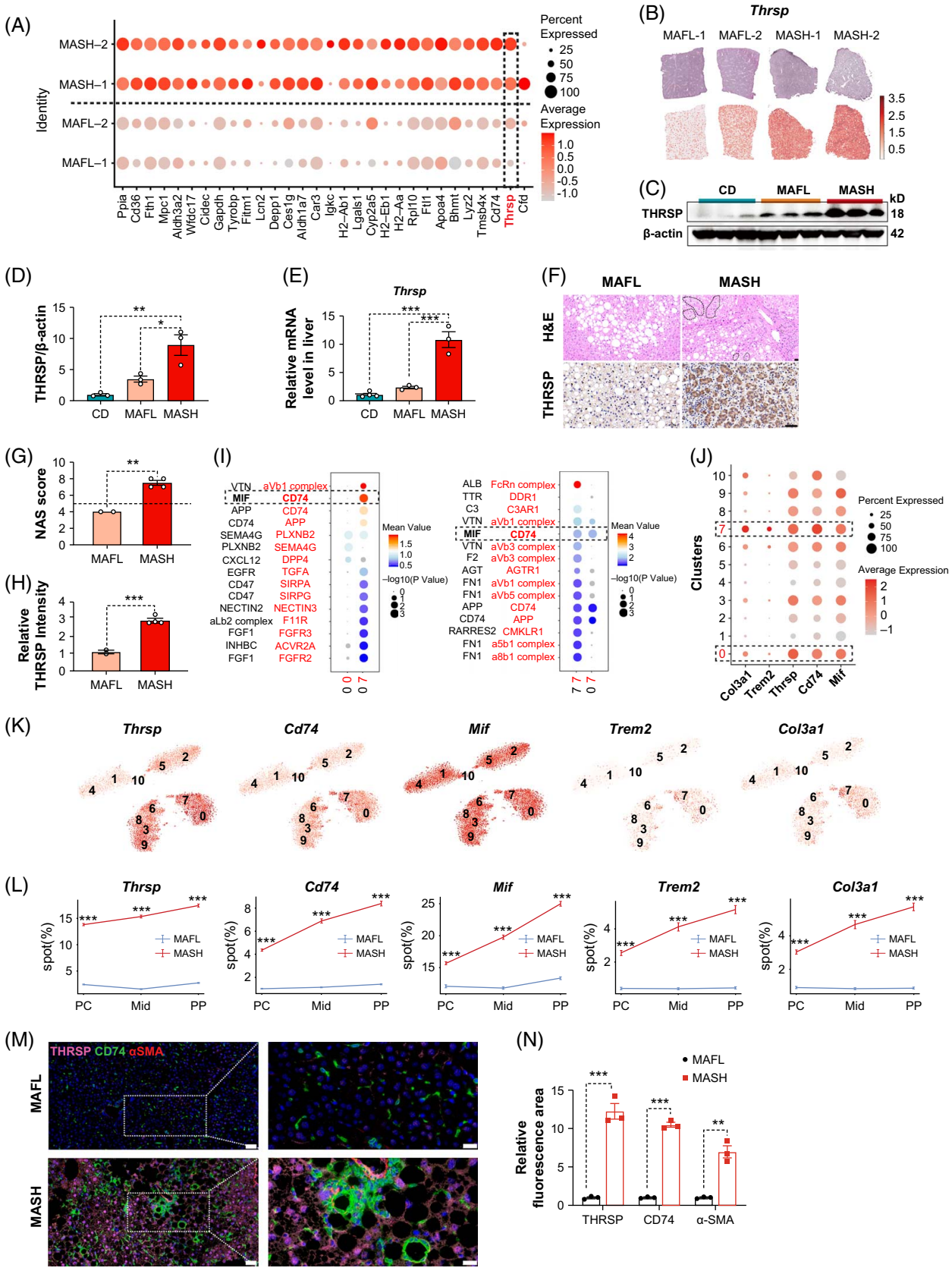

FIGURE 2 THRSP increased in MASH mice/patients and recruited CD74$^+$ LAMs in the hepatic periportal zone. (A) The bubble plot of differential genes in the livers of MAFL and MASH groups (n = 2/group, mice). The depth of color represents the average expression of the gene, and the size of the spot represents the percentage of the gene expression. (B) HE staining and *Thrsp* expression mapped onto responding tissue slices (n = 2/group, mice). (C) The protein expression levels of THRSP in livers from CD, MAFL, and MASH groups (n = 3/group, mice). (D) The quantification of C. (E) The

mRNA levels of *Thrsp* in livers from CD, MAFL, and MASH groups (n = 3/group, mice). (F) The HE staining and immunohistochemical images of THRSP expression in MAFL and MASH patients. The dotted lines indicate balloon hepatocytes in the liver section of MASH patients. Scale bars for HE and IHC were 20 μm and 50 μm, respectively. (G–H) NAS and the quantification of THRSP expression of liver sections from MAFL and MASH groups (n = 2–4/group, patients). (I) Cellphone analysis with cluster 0 and cluster 7 as ligands and receptors, respectively, with a p value < 0.05. The top 15 communication pairs based on p values are presented. The size of the spot represents the p value, while the color intensity indicates the regulatory strength of the relationship. (J) The co-location of *Thrsp*, *Cd74*, *Trem2*, and *Col3a1* in the different clusters. The dotted line outlines the colocalization results of the above genes in cluster 0 and cluster 7. (K, L) The expression and location of *Thrsp*, *Cd74*, *Mif, Trem2*, and *Col3a1* in livers as the tSNE (K) and line chart (L). N = 2/group, mice. (M, N) Representative image and quantification of mIHC in the livers from MAFL and MASH mice (more than 6 fields of 3 replicates for each group). Scale bar, 20× (50 μm) and 63× (20 μm). Data were presented as the mean ± SEM. p values were calculated by unpaired t test (G, H, N), 1-way ANOVA followed by Tukey multiple comparison test (D–E), and 2-way ANOVA followed by Tukey multiple comparison test (L). $^{*}p < 0.05$, $^{**}p < 0.01$, and $^{***}p < 0.001$. Abbreviations: CD, chow diet; HE, hematoxylin and eosin; IHC, immunohistochemistry; LAMs, lipid-associated macrophages; MAFL, metabolic dysfunction–associated fatty liver; MASH, metabolic dysfunction–associated steatohepatitis; mIHC, multiplex immunohistochemistry; NAS, NAFLD Activity Score.

indicated MAFL clusters were linked to mitochondrial morphogenesis and inhibition of gluconeogenesis, while MASH clusters were enriched in pathways related to lipoprotein particle assembly and steroid biosynthesis (Supplementary Figure S2A, http://links.lww.com/HEP/J840). These findings reinforced the biological distinction between MAFL and MASH.

Regarding zonation, we identified periportal (PP) and pericentral (PC) regions in the *t*-SNE plot using known marker genes (PC: *Oat*, PP: *Sds*)[34] (Figure 1D). MASH marker genes[38] associated with antigen processing/presentation (*Cd74*, *H2-Aa*, *H2-Ab1*), lipid-associated macrophages (LAMs) (*Trem2*, *Cd9*, *Gpnmb*), lipid metabolism (*Lpl*, *Pltp*, *Fabp7*), and fibrosis (*Mmp12*) were significantly upregulated in MASH livers compared to MAFL controls (Figure 1E). QuSAGE analysis revealed that DNL, fibrosis, inflammation, and PI3K/AKT signaling were significantly enriched in the hepatic PP zone of MASH (Figure 1F).

Moreover, ST data indicated an increase in myeloid cells, including monocytes and monocyte-derived cells, KCs (Figure 1G), cDC1s, and cDC2s (Supplemental Figures S2B, D, http://links.lww.com/HEP/J840) in the MASH PP zone. LAM markers (*Trem2*, *Gpnmb*, *Spp1*) and HSC marker *Col3a1* were notably upregulated in the MASH PP zone (Figures 1H, I). Genes related to LAMs (*Cd9*), fibrosis (*Mmp12*), FFA uptake (*Cd36*), and proliferation (*Gas6*) were expressed predominantly in the PP region in MASH mice (Supplemental Figures S3A–C, http://links.lww.com/HEP/J840). These findings highlighted the PP zone's pivotal role in inflammatory and fibrotic responses during MASH progression.

THRSP upregulation increased recruitment of CD74^{+} LAMs to the PP zone during MASH progression

Among differentially expressed genes between MAFL and MASH, *Thrsp* emerged as a key target for its role in hepatic lipogenesis[30] (Figure 2A). Analysis of sc/snRNA-seq (GSE192742) from both humans (Supplemental Figures S4A, B, http://links.lww.com/HEP/J840) and mice (Supplemental Figures S4C, D, http://links.lww.com/HEP/J840) revealed that *Thrsp* was predominantly expressed in hepatocytes. ST data revealed significantly elevated *Thrsp* expression in MASH liver compared to MAFL (Figure 2B), confirmed by RT-PCR and immunoblotting (Figures 2C–E). Additionally, histological examination of human MAFL and MASH samples, scored by NAFLD Activity Score (NAS) (Figure 2G), confirmed significantly increased THRSP expression in MASH patients (Figures 2F, H). Additionally, mIHC results demonstrated co-upregulation of THRSP and α-SMA in the MASH PP zone, suggesting an advanced fibrosis from PC to PP zones (Supplemental Figure S5, http://links.lww.com/HEP/J840). Collectively, these findings suggest that *THRSP* plays a pivotal role in MASH progression.

To explore the cell–cell communication involved in the potential mechanism of THRSP-driving MASH progression, we performed cellphone analysis in *Thrsp*-high zones (clusters 0 and 7). The bubble plot highlighted the top 15 ligand–receptor pairs between cluster 0 (ligand source) and cluster 7 (receptor target) (Figure 2I). CellPhoneDB analysis in *Thrsp*-high regions identified significant MIF-CD74 ligand–receptor interactions, with elevated *Mif* and *Cd74* expression localized in MASH PP zones. Colocalization of *Cd74*, *Thrsp*, LAMs markers (*Trem2*, *Gpnmb*), and HSC marker *Col3a1* in clusters 0 and 7 confirmed their pathological relevance (Figures 2J–L). This finding suggested that the *Thrsp*-high zone may represent a critical region of pathological dynamics during MASH progression. Additional mining of sc/snRNA-seq (GSE192742) from both humans (Supplemental Figures S4A, B, http://links.lww.com/HEP/J840) and mice (Supplemental Figures S4C–F, http://links.lww.com/HEP/J840) demonstrated that *Cd74* was predominantly expressed in hepatic macrophages and co-expressed with canonical LAMs markers (*Trem2, Cd9, Spp1, Gpnmb*, *Ms4a7*) (Supplemental Figure S4F, http://links.lww.com/HEP/J840), confirming *Cd74* was a LAMs marker. ST revealed PP zone-specific co-expression of *Thrsp* and LAMs (*Trem2*, *Gpnmb*, *Cd9*) in MASH lobules (Supplemental Figures S3D–F, http://links.lww.com/HEP/J840). These findings

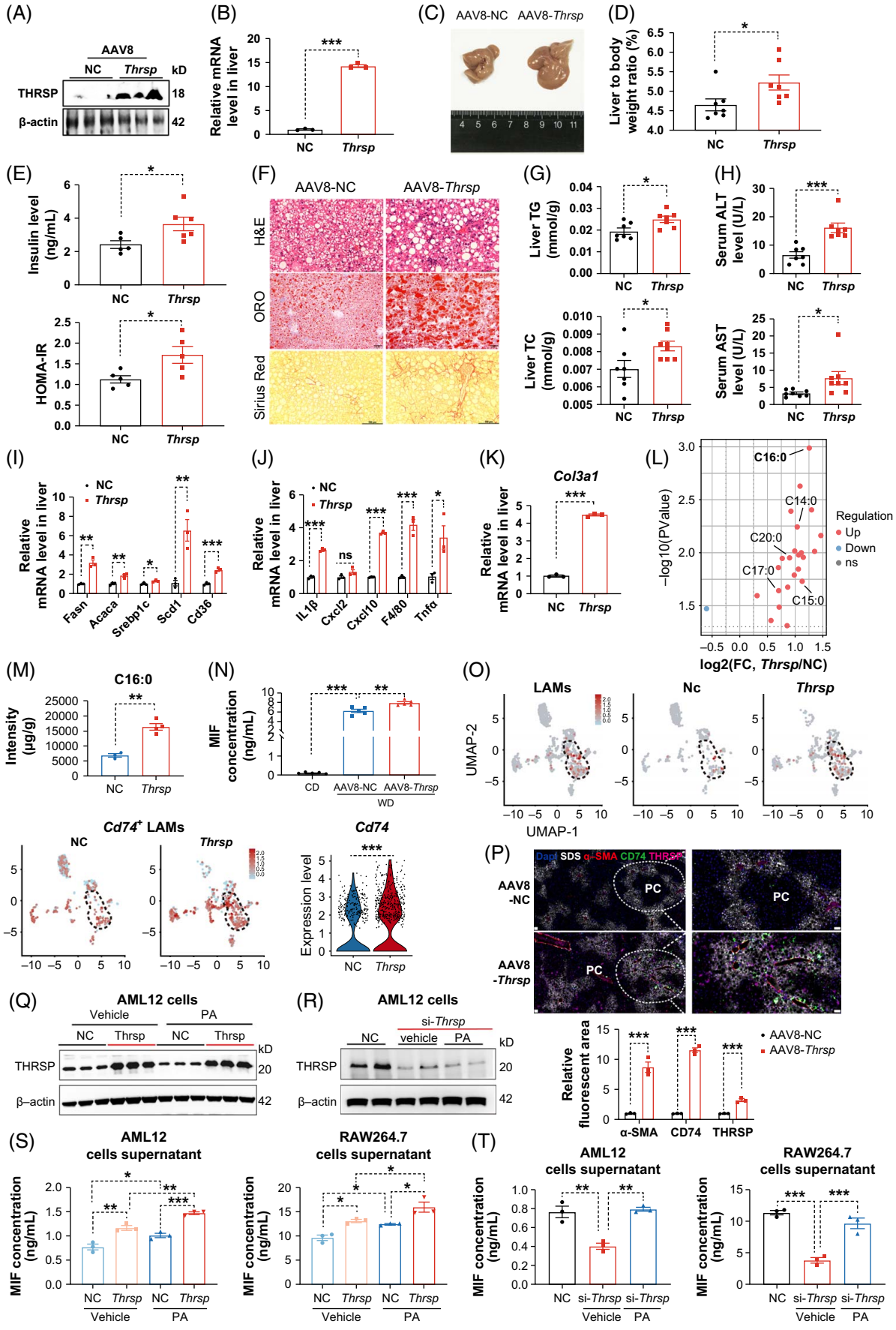
(A)
AAV8
NC
Thrsp
kD
THRSP
18
β-actin
42
(B)
Relative mRNA level in liver
NC
Thrsp
(C)
AAV8-NC
AAV8-Thrsp
(D)
Liver to body weight ratio (%)
(E)
Insulin level (ng/mL)
HOMA-IR
(F)
AAV8-NC
AAV8-Thrsp
H&E
ORO
Sirius Red
(G)
Liver TG (mmol/g)
Liver TC (mmol/g)
(H)
Serum ALT level (U/L)
Serum AST level (U/L)
(I)
Relative mRNA level in liver
Fasn
Acaca
Srebp1c
Scd1
Cd36
(J)
Il1β
Cxcl2
Cxcl10
F4/80
Tnfα
ns
(K)
Col3a1
(L)
C16:0
C14:0
C20:0
C17:0
C15:0
−log10(PValue)
log2(FC, Thrsp/NC)
Regulation
Up
Down
ns
(M)
C16:0
Intensity (μg/g)
(N)
MIF concentration (ng/mL)
CD
AAV8-NC
AAV8-Thrsp
WD
(O)
LAMs
Nc
Thrsp
UMAP-1
UMAP-2
Cd74+ LAMs
Cd74
Expression level
(P)
Dapi SDS α-SMA CD74 THRSP
AAV8 -NC
AAV8 -Thrsp
PC
Relative fluorescent area
α-SMA
CD74
THRSP
(Q)
AML12 cells
Vehicle
PA
(R)
AML12 cells
si-Thrsp
vehicle
(S)
AML12 cells supernatant
RAW264.7 cells supernatant
(T)
AML12 cells supernatant
RAW264.7 cells supernatant
si-Thrsp

FIGURE 3 AAV8-*Thrsp*-OE aggravated MASH via PA accumulation and MIF-mediated CD74$^+$ LAMs recruitment in the PP zone. (A, B) *Thrsp* OE was confirmed by WB (A) and qPCR (B) (n = 3/group, mice). (C) Representative livers, (D) liver weight to body weight ratios (n = 7/group, mice), (E) insulin levels and HOMA-IR (n = 5–6/group, mice), (F) representative H&E, ORO and sirius red staining of the liver sections, (G) liver TG and TC contents (n = 7–8/group, mice), (H) serum ALT and AST levels (n = 7–8/group, mice), (I–K) relative mRNA levels of lipogenetic and uptake genes (I), proinflammatory genes (J), and profibrotic gene (K) in livers of NC and *Thrsp*-OE mice (n = 3/group, mice). (L) The volcano map of hepatic FFA content in the NC and *Thrsp*-OE mice (n = 3/group, mice). (M) The content of palmitic acid in the NC and *Thrsp*-OE mice (n = 3–4/group, mice). (N) The serum MIF levels in the normal CD and custom WD fed NC and *Thrsp*-OE mice. (O) Our results of snRNA-seq showed expression levels of LAMs and *Cd74*$^+$ LAMs in the livers of NC and *Thrsp*-OE mice (n = 3/group, mice). (P) Representative mIHC images and responding quantification in the NC and *Thrsp*-OE mice (more than 6 fields of 3 replicates for each group). Scale bar, 50 μm. (Q, R) WB was used to confirm *Thrsp* overexpression (Q) or knockdown (R) in the AML12 cells treated with/without PA. (S, T) The MIF concentration in the culture supernatant of AML12 cells and RAW264.7 cells, which were treated with culture supernatant from anterior AML12 cells with/without PA treatment. N = 3/group. Data were presented as the mean ± SEM. *p* Values were calculated by unpaired *t* test (2 groups), 1-way ANOVA followed by Tukey multiple comparison test (≥ 3 groups). $^*p < 0.05$, $^{**}p < 0.01$, and $^{***}p < 0.001$. SDS, PP marker gene. PA, palmitic acid (PA, C16:0), 0.5 mM. Abbreviations: CD, chowdiet; FFA, free fatty acids; LAMs, lipid-associated macrophages; MASH, metabolic dysfunction–associated steatohepatitis; MIF, macrophage migration inhibitory factor; mIHC, multiplex immunohistochemistry; NC, negative control; ORO, oil red O; PP, periportal; qPCR, quantitative PCR; TC, total cholesterol; TG, triglycerides; Thrsp-OE, Thrsp-mediated overexpression; WB, western blot; WD, western diet.

collectively suggested that crosstalk between *THRSP*$^+$ *hepatocytes* and CD74$^+$ LAMs in the PP zone played a vital role in MASH progression.

Our findings suggested THRSP (hepatocyte-derived) and CD74 (LAMs-specific) mediated hepatocyte–macrophage crosstalk during MASH progression, potentially through lipid-driven activation pathways.[19] mIHC and the quantification analyses revealed increased CD74 and THRSP expression in MASH livers, with CD74 forming crown-like structures around lipid droplets (Figures 2M, N). Based on the above results, lipids may serve as crucial mediators in recruiting CD74$^+$ LAMs during the THRSP-facilitated MASH process.

Hepatocyte THRSP exacerbated MASH via PA accumulation and MIF-dependent CD74$^+$ LAMs recruitment in the PP zone

Lipotoxicity is a chief trigger of hepatocyte injury in MASH.[45,46] Given the established role of THRSP in promoting hepatic lipogenesis and its marked upregulation during MAFL-to-MASH transition, we generated hepatocyte-specific *Thrsp*-overexpressing mice (*Thrsp* OE) to investigate its direct contribution to MASH progression. WB and RT-PCR analyses validated successful *Thrsp* OE in the livers of AAV8-*Thrsp*-injected mice (Figures 3A, B). *Thrsp*-OE mice exhibited significantly increased liver weight, liver-to-body weight ratios (Figures 3C, D), and insulin resistance (Figure 3E) compared to controls, with minimal changes in overall body weight (Supplemental Figure 6A, http://links.lww.com/HEP/J840). Furthermore, these mice demonstrated increased lipid accumulation, inflammation, fibrosis, and liver injury relative to controls (Figures 3F–K), indicating that *THRSP* served as a crucial driver of MASH progression.

Next, to identify the specific mediators involved in *THRSP*-driven MASH progression, we focused on hepatic lipotoxicity, primarily caused by SFFA. *Thrsp* OE mice showed elevated long-chain fatty acids (LCFAs) in WD-induced MASH. Notably, quantitative profiling revealed that PA accumulation was the most pronounced among all saturated fatty acids in *Thrsp*-OE livers (Figures 3L, M, and Supplemental Figure S7, http://links.lww.com/HEP/J840). SFFA and USFFA were categorized according to their double bond counts (Supplemental Figures S7B, C, http://links.lww.com/HEP/J840). Previous studies had reported that SFFA, particularly PA, exhibited more severe lipotoxicity than USFFA, often leading to increased cell death.[12–14] Therefore, we speculated that THRSP-synthesized PA played a central role in the cellular communication between THRSP and CD74$^+$ LAMs. Based on prior cell communication findings indicating enhanced MIF/CD74 interactions in regions with high expression of *Thrsp*, we investigated THRSP's role in MIF secretion in vivo. The serum MIF content was significantly elevated in the MASH mice, and *Thrsp* OE further increased MIF release (Figure 3N). Moreover, our snRNA-seq results discovered that the proportions of LAMs (markers: *Trem2*, *Gpnmb*) and *Cd74*$^+$ LAMs were significantly increased in the livers from *Thrsp* OE mice compared to *Thrsp*-NC mice (Figure 3O and Supplemental Figures 8A, B, http://links.lww.com/HEP/J840). Pathway enrichment analysis indicated MAPK activity, immune effector process, fatty acid transport, and chemotaxis were significantly upregulated in the hepatocytes of *Thrsp*-OE mice (Supplemental Figure S8C, http://links.lww.com/HEP/J840). In the hepatic macrophages of *Thrsp*-OE mice, taxis, inflammation-related stress-activated MAPK cascade, NF-κB signaling, and fatty acid metabolism were significantly upregulated (Supplemental Figure S8D, http://links.lww.com/HEP/J840). Based on these results, which suggested that fatty acids played a significant role in the cellular communication between hepatocytes and macrophages. Moreover, mIHC results demonstrated that *Thrsp* OE led to an increase of CD74$^+$ LAMs and fibrosis in the hepatic PP zone of MASH mice (Figure 3P).

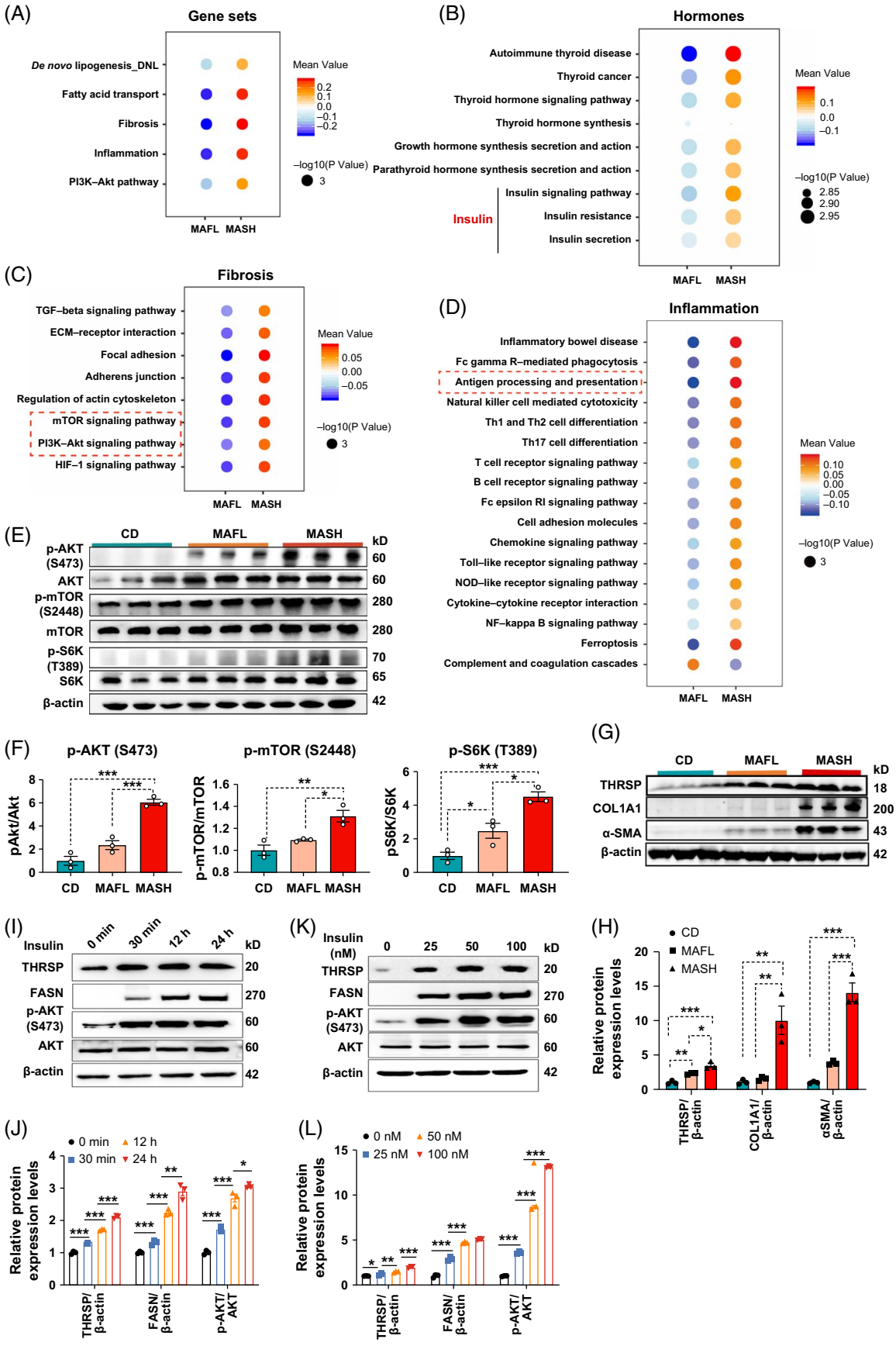
(A)
Gene sets
De novo lipogenesis_DNL
Fatty acid transport
Fibrosis
Inflammation
PI3K–Akt pathway
MAFL MASH
Mean Value
0.2
0.1
0.0
−0.1
−0.2
−log10(P Value)
3
(B)
Hormones
Autoimmune thyroid disease
Thyroid cancer
Thyroid hormone signaling pathway
Thyroid hormone synthesis
Growth hormone synthesis secretion and action
Parathyroid hormone synthesis secretion and action
Insulin
Insulin signaling pathway
Insulin resistance
Insulin secretion
MAFL MASH
Mean Value
0.1
0.0
−0.1
−log10(P Value)
2.85
2.90
2.95
(C)
Fibrosis
TGF–beta signaling pathway
ECM–receptor interaction
Focal adhesion
Adherens junction
Regulation of actin cytoskeleton
mTOR signaling pathway
PI3K–Akt signaling pathway
HIF–1 signaling pathway
MAFL MASH
Mean Value
0.05
0.00
−0.05
−log10(P Value)
3
(D)
Inflammation
Inflammatory bowel disease
Fc gamma R–mediated phagocytosis
Antigen processing and presentation
Natural killer cell mediated cytotoxicity
Th1 and Th2 cell differentiation
Th17 cell differentiation
T cell receptor signaling pathway
B cell receptor signaling pathway
Fc epsilon RI signaling pathway
Cell adhesion molecules
Chemokine signaling pathway
Toll–like receptor signaling pathway
NOD–like receptor signaling pathway
Cytokine–cytokine receptor interaction
NF–kappa B signaling pathway
Ferroptosis
Complement and coagulation cascades
MAFL MASH
Mean Value
0.10
0.05
0.00
−0.05
−0.10
−log10(P Value)
3
(E)
CD MAFL MASH
kD
p-AKT (S473) 60
AKT 60
p-mTOR (S2448) 280
mTOR 280
p-S6K (T389) 70
S6K 65
β-actin 42
(F)
p-AKT (S473)
pAkt/Akt
CD MAFL MASH
p-mTOR (S2448)
p-mTOR/mTOR
CD MAFL MASH
p-S6K (T389)
pS6K/S6K
CD MAFL MASH
(G)
CD MAFL MASH
kD
THRSP 18
COL1A1 200
α-SMA 43
β-actin 42
(H)
CD
MAFL
MASH
Relative protein expression levels
THRSP/β-actin
COL1A1/β-actin
αSMA/β-actin
(I)
Insulin 0 min 30 min 12 h 24 h
kD
THRSP 20
FASN 270
p-AKT (S473) 60
AKT 60
β-actin 42
(J)
0 min 12 h
30 min 24 h
Relative protein expression levels
THRSP/β-actin
FASN/β-actin
p-AKT/AKT
(K)
Insulin (nM) 0 25 50 100
kD
THRSP 20
FASN 270
p-AKT (S473) 60
AKT 60
β-actin 42
(L)
0 nM 50 nM
25 nM 100 nM
Relative protein expression levels
THRSP/β-actin
FASN/β-actin
p-AKT/AKT

FIGURE 4 THRSP responded to insulin, and the PI3K/AKT/mTOR signaling pathway was activated in MASH. (A–D) Gene set analyses in the livers from MAFL and MASH mice. (E) WB was used to confirm the activation of the AKT/mTOR signaling pathway in MASH mice. (F) The quantification of E (n = 3/group, mice). (G) WB was used to confirm the upregulation of THRSP and fibrosis-related proteins in MASH. (H) The quantification of G (n = 3/group, mice). (I, K) The protein expressions of THRSP, FASN, and p-AKT in the AML12 cells treated with insulin at different time points (I) and doses (K). (J, L) The quantifications of I and K (n = 3). Data were presented as the mean ± SEM. All statistical analyses were carried out by one-way ANOVA followed by the Tukey multiple comparison test. *$p < 0.05$, **$p < 0.01$, and ***$p < 0.001$. Abbreviations: CD, control diet; FASN, fatty acid synthase; MAFL, metabolic dysfunction–associated fatty liver; MASH, metabolic dysfunction–associated steatohepatitis; WB, western blot.

To confirm whether PA was the key molecular mediator facilitating communication between THRSP and CD74$^+$ LAMs, we conducted co-culture experiments involving hepatocytes (AML12 cells) and macrophages (RAW264.7 cells). Conditioned media from *Thrsp*-OE AML12 cells (Figure 3Q) increased MIF secretion both in hepatocytes and macrophages, regardless of PA stimulation, suggesting that THRSP promoted CD74$^+$ LAMs activation. Additionally, compared to the groups without PA, the addition of PA further increased MIF release, suggesting PA enhanced CD74$^+$ LAMs activation (Figure 3S). Rescue experiments showed that PA restored the reduced secretion levels of MIF caused by *Thrsp* knockdown both in hepatocytes and macrophages (Figure 3R, T). Taken together, our results are convincing that PA-induced MIF release from hepatocytes and macrophages was the specific mediator of crosstalk between THRSP and CD74$^+$ LAMs.

THRSP responded to insulin, and the PI3K/AKT/mTOR signaling pathway was activated in MASH mice

To elucidate the underlying molecular mechanisms of THRSP promoting FFA synthesis, we performed QuSAGE analysis utilizing the KEGG database to assess alterations of the transcriptional profile in livers from MAFL and MASH mice. Gene set enrichment analysis showed significant enrichment of gene sets related to the PI3K/AKT/mTOR pathway, DNL, inflammation, and fibrosis in the livers of MASH mice (Figure 4A). Next, we focused on the enriched gene sets associated with hormones, inflammation, and fibrosis, and found significant enrichment of thyroid hormone, insulin signaling pathways, PI3K/AKT/mTOR pathway, and antigen presentation-related gene sets (Figures 4B–D). We further validated PI3K/AKT/mTOR pathways (Figures 4E, F) and the enriched fibrosis-related proteins by WB assays (Figures 4G, H).

Given insulin's critical role in promoting DNL in the liver,[47] we investigated whether THRSP acted as an insulin-responsive protein. We detected THRSP expression in AML12 cells treated with insulin by WB. Remarkably, insulin stimulation increased THRSP, FASN, and p-AKT levels in a dose-dependent and time-dependent manner (Figures 4I–L). All these results demonstrated that the THRSP protein level was increased following insulin treatment, and key genes in DNL and PI3K/AKT/mTOR pathways showed coordinated upregulation in MASH.

THRSP promoted lipogenesis by activating the AKT/mTOR pathway and enhancing FASN protein stability

To clarify THRSP's role in lipogenesis, we performed gain-of-function and loss-of-function experiments in murine primary hepatocytes using ORO staining. *Thrsp* OE promoted lipid accumulation, while *Thrsp* inhibition via siRNA reduced lipogenesis (Figures 5A, B). Given that *THRSP* was an insulin-responsive protein, we assessed its dependence on insulin for lipogenic effects. Stable THRSP overexpression in AML12 cells activated AKT/mTOR signaling and increased FASN expression independently of insulin. To validate whether the activation of AKT/mTOR signaling pathway by THRSP was insulin dependent, we employed 2 AKT inhibitors (AKTi mix) (Supplemental Figure S9, http://links.lww.com/HEP/J840). AKT inhibition suppressed mTOR signaling, FASN, and THRSP expressions (Figures 5C–F), demonstrating THRSP's dual regulation of lipogenesis through both insulin-dependent and insulin-independent manners.

Subsequently, we explored the mechanism of THRSP in promoting FFA synthesis by insulin-independent FASN induction. To assess the interaction between THRSP and FASN in vivo, we conducted IF assays. Interestingly, colocalization efficiency between THRSP and FASN was elevated in *Thrsp*-OE MASH mice (Figures 5G, H). Co-IP assays confirmed THRSP–FASN binding, which increased with *Thrsp* OE and decreased upon AKT inhibition (Figure 5I). Following transient transfection (*Thrsp*-Flag or empty vector), CHX-treated AML12 cells showed THRSP-dependent FASN stabilization by WB (Figure 5J). Notably, the half-life of FASN protein was significantly extended in the *Thrsp*-transfected cells (Figure 5K).

THRSP competitively bound to FASN and TRIM21, disrupted the TRIM21–FASN interaction, and enhanced FASN protein stability

To identify THRSP-interacting proteins mediating FASN stabilization, we performed anti-THRSP

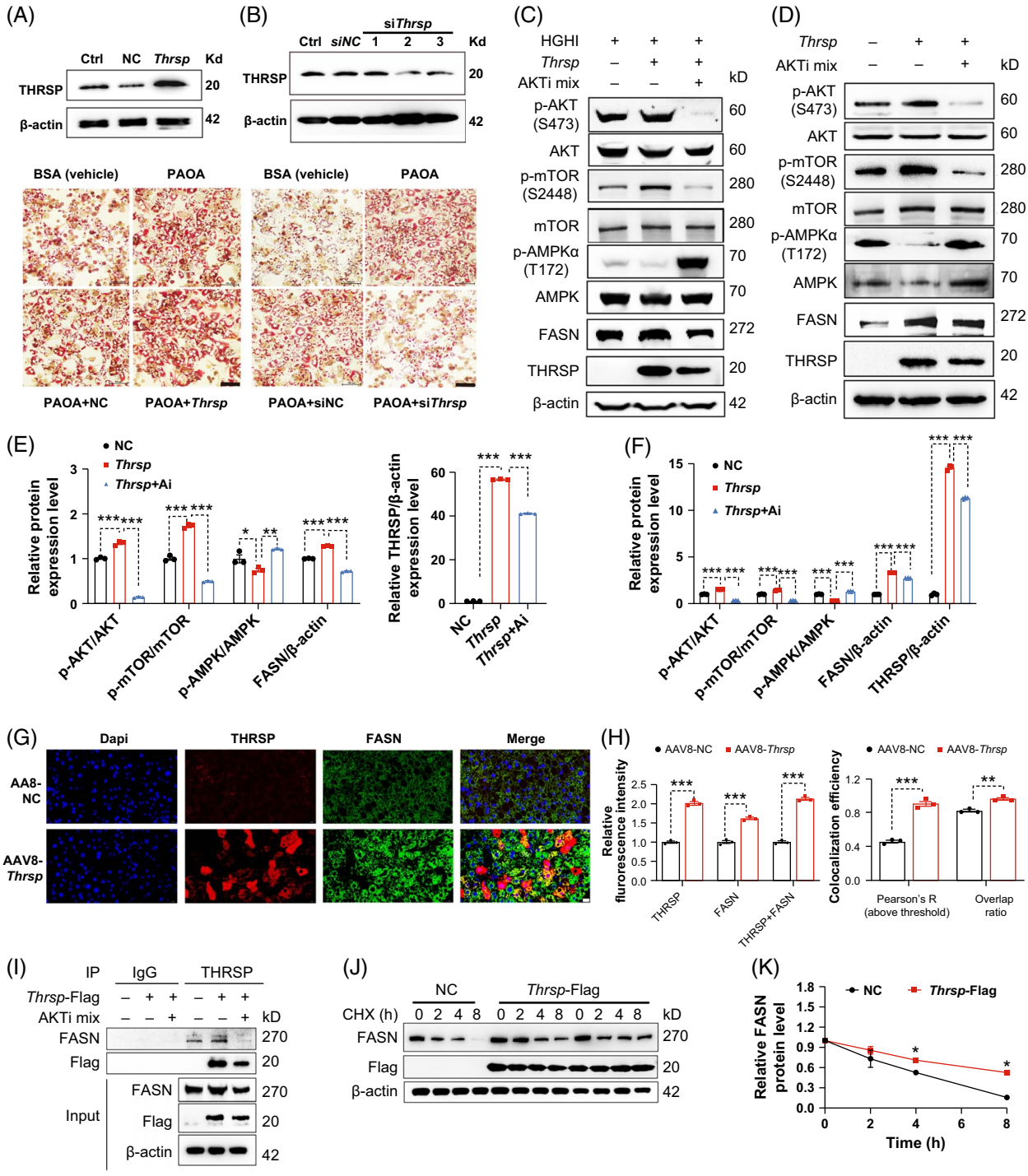

FIGURE 5 THRSP increased hepatic lipogenesis by activating AKT/mTOR signaling pathway and enhancing FASN protein stability. (A, B) WB was used to confirm the *Thrsp* overexpression and knockdown by siRNA. Representative Oil Red O staining in the primary hepatocytes of the indicated groups (more than 6 fields of 3 replicates for each group). Scale bars, 100 μm. (C, D) The expressions of the indicated proteins in the *Thrsp*-transfected AML12 cells treated with (A) or without (B) HGHI. (E, F) The quantification of A and B (3 independent experiments conducted). (G) The expressions of THRSP and FASN co-expressed in the livers of the indicated groups. Scale bar, 20 μm. (H) The quantification of G and the colocalization efficiency (Pearson *R*, overlap ratio) between THRSP and FASN (more than 6 fields of 3 biological replicates for each group). (I) Co-IP assay revealing the interaction of THRSP and FASN. (J, K) FASN expression and quantification in the indicated groups. Data were presented as the mean ± SEM. All statistical analyses were carried out by 1-way ANOVA followed by Tukey multiple comparison test (E, F), 2-way ANOVA followed by Sidak multiple comparison test (K), and unpaired *t* test (H). $^{**}p < 0.01$, and $^{***}p < 0.001$. Abbreviations: AKTi mix, AKT inhibitor mixtures; HGHI, high glucose (30 mM) and high insulin (100 nM). CHX, cycloheximide (10 μM). Co-IP, co-immunoprecipitation; FASN, fatty acid synthase.

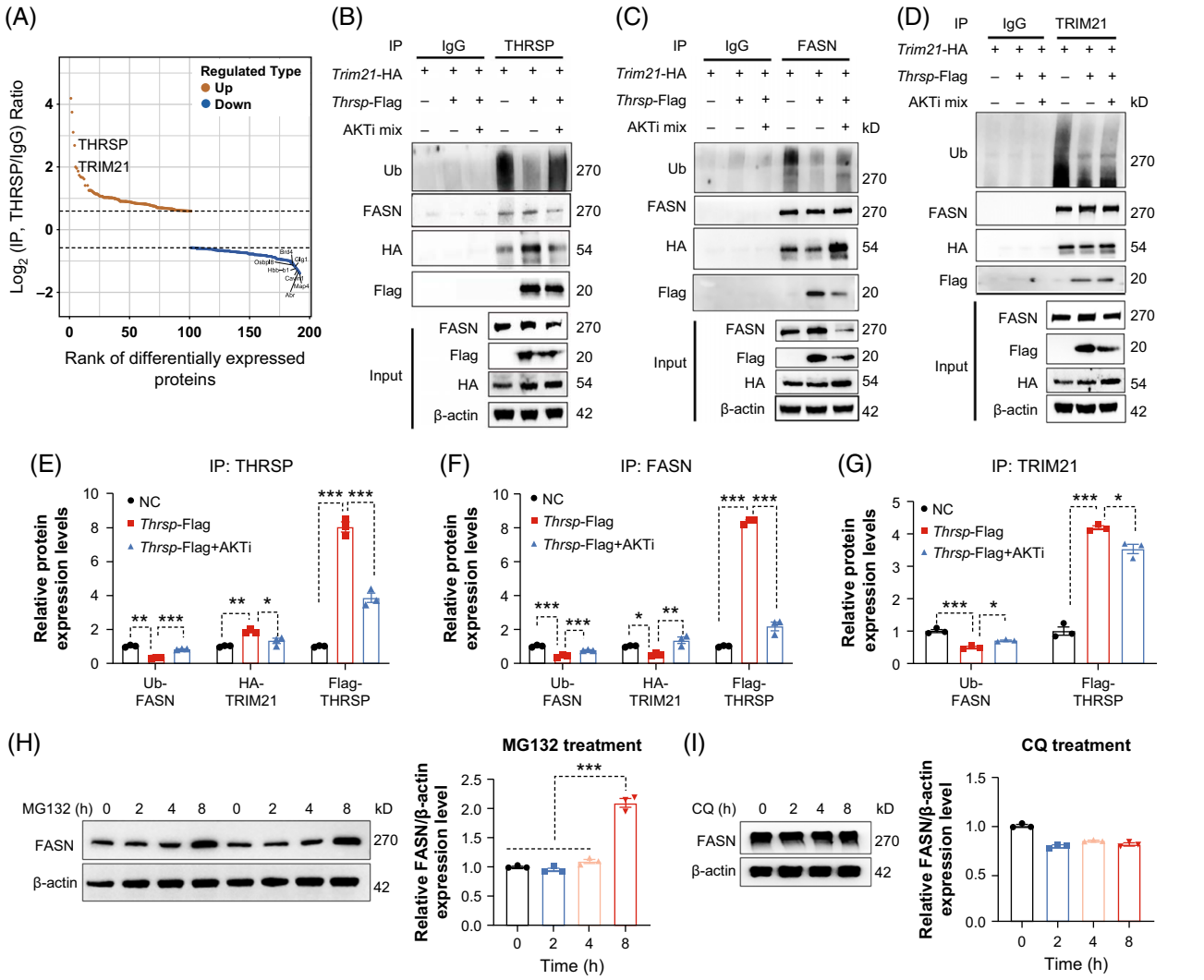

FIGURE 6 THRSP competitively bound to FASN and TRIM21 and inhibited the ubiquitination of FASN by TRIM21. (A) IP/MS assay showing the interacted proteins with THRSP from anti-IgG or anti-THRSP immunoprecipitate in the *Thrsp* overexpressed AML12 cells, IgG was used as an isotype control. (B–D) Co-immunoprecipitation assay showing the interaction of THRSP, FASN, and TRIM21 as indicated in the immunoblot of anti-THRSP (B), anti-FASN (C), or anti-TRIM21 (D) immunoprecipitate and whole cell lysate (input) from AML12 cells transfected with the indicated plasmids and treated with or without AKTi mix. (E) The quantification of B. (F) The quantification of C. (G) The quantification of D. (H) Immunoblot and quantification of FASN in AML12 cells with MG132 (10 μM) treatment. (I) Immunoblot and quantification of FASN in AML12 cells with Chloroquine (CQ, 10 μM) treatment. All statistical analyses were carried out by one-way ANOVA followed by the Tukey multiple comparison test. *$p < 0.05$, **$p < 0.01$, and ***$p < 0.001$. Abbreviations: BSA, bovine serum albumin; FASN, fatty acid synthase; NC, negative control; OA, oleic acid; PA, palmitic acid; IP/MS, immunoprecipitation coupled with mass spectrometry.

immunoprecipitation coupled with mass spectrometry (IP–MS) in *Thrsp*-OE AML12 cells. Among the identified candidates, TRIM21, a well-known E3 ubiquitin ligase, was prominently noted (Figure 6A). Therefore, we investigated the interactions among THRSP, FASN, and TRIM21. Co-IP results demonstrated that *Thrsp* OE reduced FASN ubiquitination and enhanced THRSP–FASN and THRSP–TRIM21 binding (Figures 6B–G). These findings suggested that, under conditions of THRSP-OE, THRSP enhanced the stability of the FASN protein by disrupting TRIM21–FASN binding. FASN accumulation following the proteasome inhibitor MG132 (Figure 6H) but not autophagy inhibitor chloroquine (CQ) treatment (Figure 6I) implicated the ubiquitin–proteasome system as the dominant degradation pathway. Our results suggested that THRSP competitively bound to FASN and TRIM21, inhibiting TRIM21-mediated ubiquitination of FASN, thereby enhancing its protein stability.

Hepatocyte-specific *Thrsp* knockout (*Thrsp*-HKO)/knockdown ameliorated MASH by reducing hepatic PA content and MIF-mediated CD74$^+$ LAMs recruitment in the PP zone

Then, we assessed the therapeutic efficacy of hepatocyte-specific *Thrsp*- HKO/knockdown in MASH. The

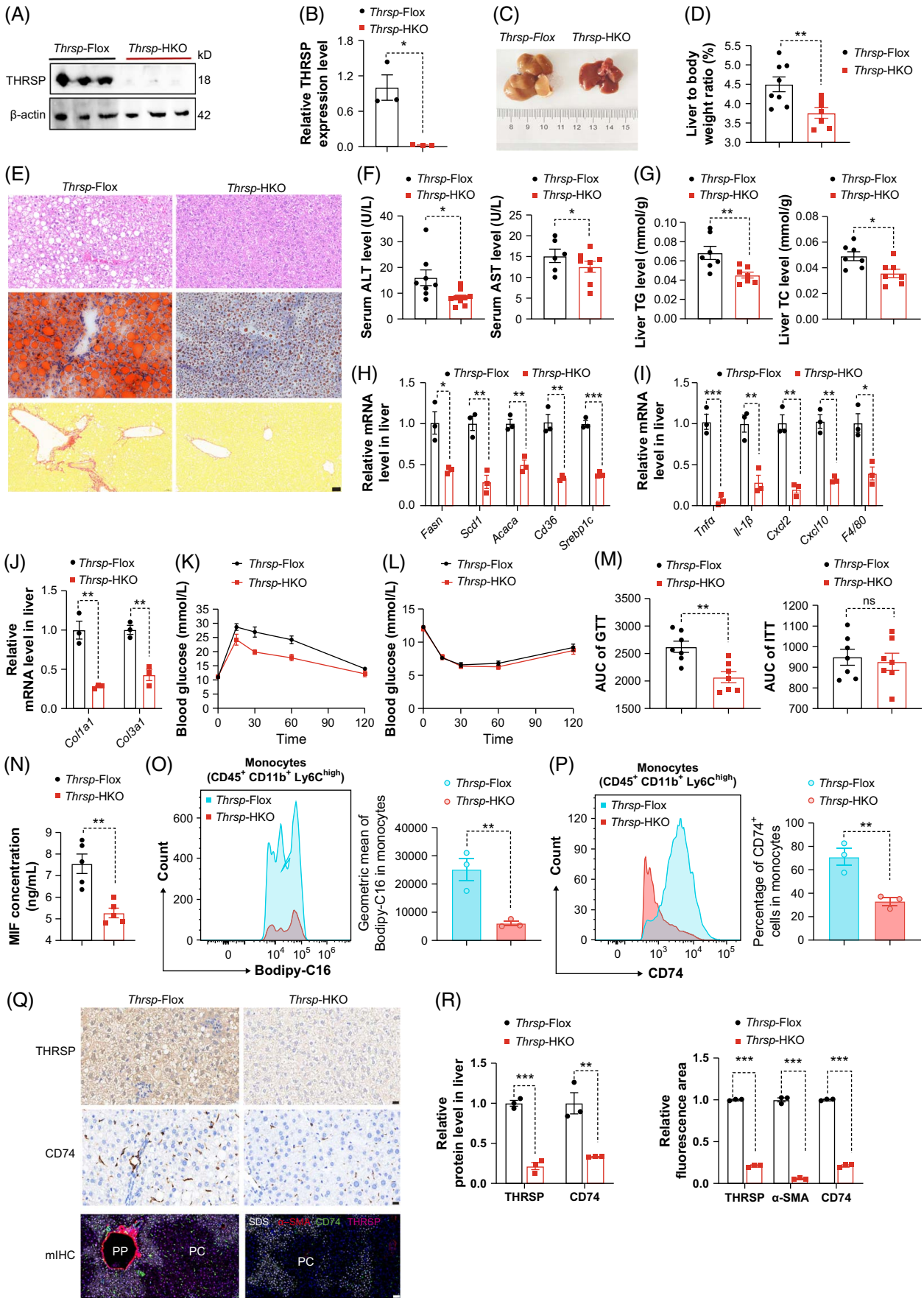
(A)
Thrsp-Flox
Thrsp-HKO
kD
THRSP
18
β-actin
42
(B)
Thrsp-Flox
Thrsp-HKO
Relative THRSP expression level
(C)
Thrsp-Flox
Thrsp-HKO
(D)
Liver to body weight ratio (%)
(E)
Thrsp-Flox
Thrsp-HKO
(F)
Serum ALT level (U/L)
Serum AST level (U/L)
(G)
Liver TG level (mmol/g)
Liver TC level (mmol/g)
(H)
Relative mRNA level in liver
Fasn
Scd1
Acaca
Cd36
Srebp1c
(I)
Relative mRNA level in liver
Tnfα
Il-1β
Cxcl2
Cxcl10
F4/80
(J)
Relative mRNA level in liver
Col1a1
Col3a1
(K)
Blood glucose (mmol/L)
Time
(L)
Blood glucose (mmol/L)
Time
(M)
AUC of GTT
AUC of ITT
ns
(N)
MIF concentration (ng/mL)
(O)
Monocytes (CD45+ CD11b+ Ly6Chigh)
Count
Bodipy-C16
Geometric mean of Bodipy-C16 in monocytes
(P)
Monocytes (CD45+ CD11b+ Ly6Chigh)
Count
CD74
Percentage of CD74+ cells in monocytes
(Q)
Thrsp-Flox
Thrsp-HKO
THRSP
CD74
mIHC
PP
PC
PC
SDS α-SMA CD74 THRSP
(R)
Relative protein level in liver
THRSP
CD74
Relative fluorescence area
THRSP
α-SMA
CD74

FIGURE 7 Hepatocyte-specific *Thrsp*-HKO mice ameliorated MASH by reducing hepatic PA content and CD74$^+$ LAMs recruitment mediated by MIF in the PP zone. (A) Representative livers, (B) liver-to-body weight ratio, (C) THRSP protein expression level, (D) the quantification of C, (E) representative H&E, Oil Red O (ORO), and sirius red staining of the liver sections, (F) serum ALT (left) and AST (right), (G) liver TG (left) and TC (right), relative mRNA levels of lipogenetic and uptake genes (H), proinflammatory genes (I), and profibrotic gene (J) in livers, (K) GTT, (L) ITT, (M) the AUC quantification of GTT and ITT from *Thrsp*-Flox and *Thrsp*-HKO mice fed with custom WD (modified western diet containing 40% kcal from fat and 0.2% cholesterol along with a high fructose–glucose solution) for 16 weeeks. (N) The serum MIF contents of *Thrsp*-Flox and *Thrsp*-HKO mice. (O, P) Flow cytometry analysis of liver monocytes stained with BODIPY-C16 (O) and CD74 (P), respectively, in *Thrsp*-Flox and *Thrsp*-HKO mice. (Q) Representative IHC staining (scale bar, 20 μm) and (Q) mIHC images (scale bar, 50 μm) in *Thrsp*-Flox and *Thrsp*-HKO mice. (R) The quantification of Q. Data were presented as the mean ± SEM. All statistical analyses were carried out by an unpaired *t* test. $^*p < 0.05$, $^{**}p < 0.01$, and $^{***}p < 0.001$. Abbreviations: GTT, glucose tolerance test; H&E, hematoxylin and eosin; IHC, immunohistochemistry; ITT, insulin tolerance test; LAMs, lipid-associated macrophages; MASH, metabolic dysfunction–associated steatohepatitis; MIF, macrophage migration inhibitory factor; mIHC, multiplex immunohistochemistry; ORO, oil red O; PA, palmitic acid; SDS, periportal (PP) marker gene; TC, total cholesterol; TG, triglycerides; Thrsp-HKO, thrsp knockout; WD, western diet.

knockout/knockdown of *Thrsp* was confirmed in the livers (Figures 7A, B, and Supplemental Figures S10A, B, http://links.lww.com/HEP/J840). *Thrsp*-HKO/knockdown exhibited a significant reduction in liver weights and liver-to-body weight ratios, lipid accumulation, inflammation, fibrosis, liver injury, and improved glucose tolerance, with minimal impact on body weight (Figures 7C–M and Supplemental Figure S6B, http://links.lww.com/HEP/J840 and Supplemental Figures S10C–K, http://links.lww.com/HEP/J840). *Thrsp* knockdown lowered hepatic LCFAs levels, particularly PA (Supplementary Figure S10L, http://links.lww.com/HEP/J840 and Supplemental Figure S11, http://links.lww.com/HEP/J840). The serum MIF content was significantly decreased in the *Thrsp*-HKO mice (Figure 7N). Meanwhile, flow cytometry results confirmed that compared to *Thrsp*-Flox, *Thrsp*-HKO significantly reduced PA content and CD74$^+$ cells percentage in hepatic monocytes (Figures 7O, P and Supplemental Figure S12, http://links.lww.com/HEP/J840). The IHC data revealed that *Thrsp*-HKO significantly decreased THRSP and CD74 protein levels in livers (Figures 7Q, R). Furthermore, *Thrsp*-HKO/knockdown significantly reduced CD74 level and fibrosis in the hepatic PP zone (Figures 7Q, R and Supplemental Figures S10M, N, http://links.lww.com/HEP/J840). Our results uncovered that *Thrsp*-HKO/knockdown ameliorated MASH by reducing PA content and MIF-mediated recruitment of CD74$^+$ LAMs in the hepatic PP zone.

Compound C6 improved the WD-induced MASH in mice

To explore the possibility of THRSP as a therapeutic target, we performed a high-throughput virtual screen of 71,100 small molecules, selecting 6 candidates for experimental validation, as outlined in the screening workflow (Figure 8A). Of these, compound C6 markedly reduced *THRSP* protein levels (Figure 8B) without cytotoxicity in AML12 cells (Figure 8C). Molecular docking analysis further supported a binding interaction between C6 and the THRSP protein (Figure 8D). Biophysical (CETSA) and biochemical (WB) evidence established C6 as a THRSP-stabilizing ligand through direct binding (Figure 8E). Collectively, these results indicated that C6 acted as a candidate for a *THRSP* inhibitor.

In WD-fed MASH mice, C6 and resmetirom (Res) treatment decreased THRSP protein level (Figure 8F), concomitantly improving glucose/insulin tolerance (Figures 8G, H), decreasing liver triglycerides (TG), total cholesterol (TC) (Figure 8I), liver-to-body weight ratios (Figure 8J), and body weights (Figure 8K). C6 and Res treatment attenuated MASH histopathology (steatosis, inflammation, fibrosis) by H&E/Sirius Red staining, while downregulating THRSP and CD74 expression levels in liver tissue (Figure 8L). Our results revealed that C6 dose-dependently improved body weight, hepatic TC, and insulin tolerance, while also dose-dependently decreased the expressions of THRSP and CD74, suggesting that THRSP was an important target for MASH therapy. Additionally, in vivo experimental results demonstrated that C6 significantly ameliorated MASH in *Thrsp*-Flox mice, but failed to improve the MASH phenotype in *Thrsp*-HKO mice (Supplemental Figures S13A–E, http://links.lww.com/HEP/J840). Similarly, in vitro ORO assay revealed that C6 markedly alleviated intrahepatic lipid accumulation induced by PO, yet it did not reduce the lipid content in the AML12 cells following knockdown of *Thrsp* (Supplemental Figures S13F, G, http://links.lww.com/HEP/J840). Collectively, these findings indicated that the amelioration of MASH by C6 was dependent on THRSP. To further evaluate the safety profile of C6, serum levels of ALT, AST, and creatinine were measured, showing improved liver function with no adverse effects on kidney function (Figure 8M). In summary, our results highlighted that C6 was a promising THRSP inhibitor for MASH treatment.

DISCUSSION

LAMs clearly accelerate MAFL–MASH progression, yet their underlying mechanisms remain elusive. Our multi-omics approach (ST, snRNA-seq, lipidomics)

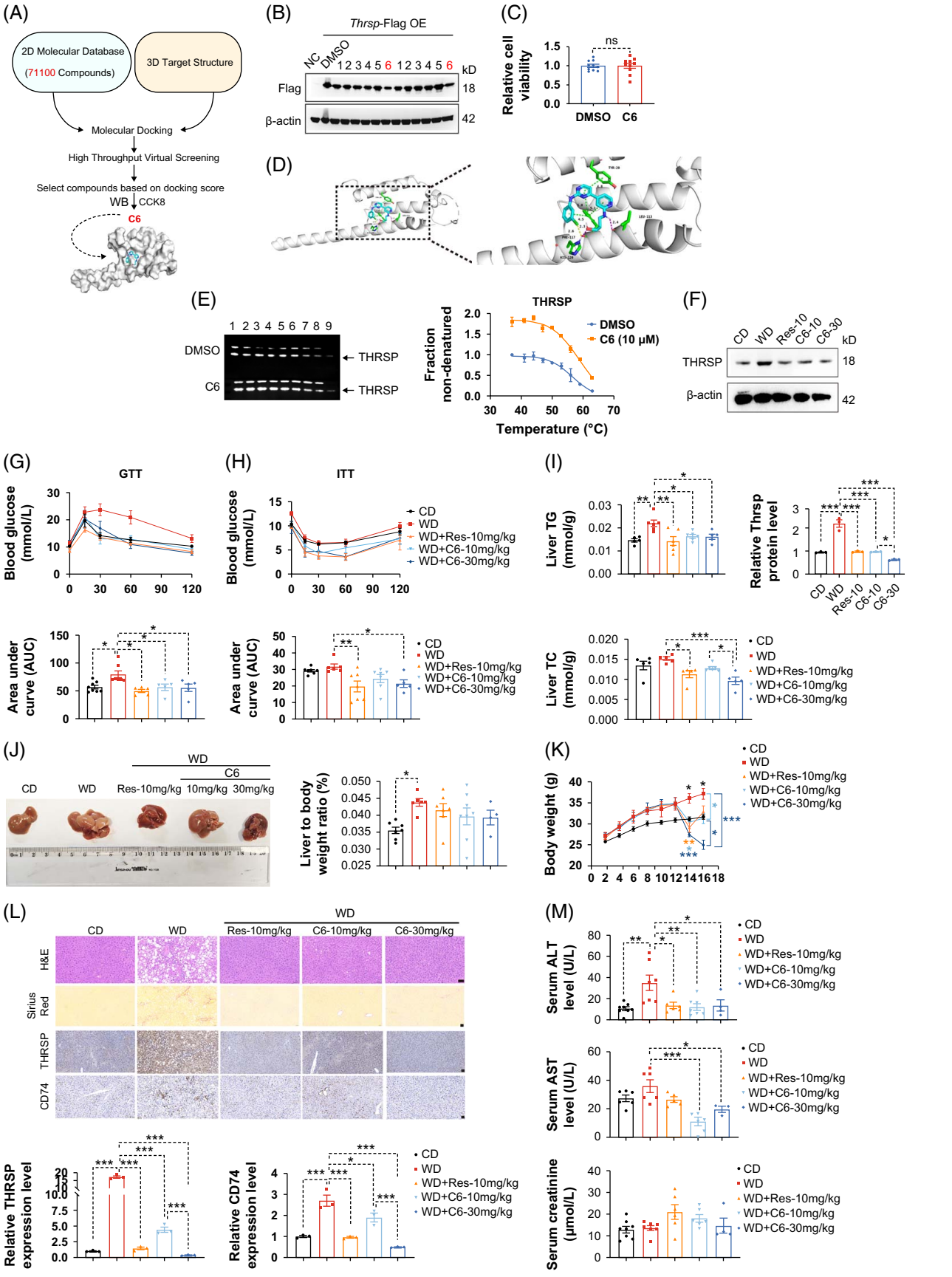

FIGURE 8 C6 screened by targeting THRSP significantly improved MASH. (A) The screening workflow of the lead compound for the THRSP inhibitor. (B) The protein levels of THRSP with different compound treatments. (C) The cell viability in the indicated groups (n = 10). (D) The

molecular docking of C6 with THRSP. (E) The WB and quantitative curve of non-denatured THRSP under thermal stimulation at 37° C, 41°C, 44° C, 47°C, 50°C, 53°C, 56°C, 59°C, and 63°C (bands: 1–9) under DMSO or compound C6 treatment conditions (3 technical replicates). (F) WB was used to detect the effects of Res (10 mg/kg) and C6 (10, 30 mg/kg) on the THRSP protein level. (G) GTT and the AUC in the indicated groups (n = 4–7/group, mice). (H) ITT and the AUC in the indicated groups (n = 4–7/group, mice). (I) Liver TG and TC in the indicated groups (n = 4–5/group, mice). (J) The liver and liver-to-body weight ratio in the indicated groups. (K) The body weight in the indicated groups (n = 4–8/group, mice). (L) HE, Sirius Red, IHC staining, and their quantifications in the indicated groups (n = 3/group, mice). Scale bars, 50 μm. (M) The serum ALT, AST, and creatinine levels in the indicated groups (4–8/group, mice). Data were presented as the mean ± SEM. All statistical analyses were carried out by unpaired *t* test (C), 1-way ANOVA followed by the Tukey multiple comparison test (F–J, L, M), 2-way ANOVA followed by Sidak multiple comparison test (K), $*p < 0.05$, $**p < 0.01$, and $***p < 0.001$. Abbreviations: CD, control diet; GTT, glucose tolerance test; IHC, immunohistochemistry; ITT, insulin tolerance test; MASH, metabolic dysfunction–associated steatohepatitis; NC, negative control; Res, Resmetirom; TC, total cholesterol; TG, triglycerides; THRSP, thyroid hormone-responsive protein; WB, western blot; WD, western diet.

delineated spatially resolved liver zonation in MAFL–MASH progression, identifying THRSP as a central driver. Mechanistically, THRSP recruits $CD74^+$ LAMs via PA-induced MIF secretion, particularly in the PP zone, driving steatohepatitis through hepatocyte–macrophage crosstalk. This PP zone-specific THRSP–MIF–CD74 axis offers a therapeutic target for precision intervention in MASH.

Given liver heterogeneity, single-cell sequencing and ST techniques provide valuable insights into the liver's cellular and tissue architecture, particularly under pathological and physiological conditions.[48] Our ST analysis identifies the PP zone as a critical niche for myeloid cell accumulation in MASH, with LAMs showing predominant enrichment. Functional enrichment analyses demonstrate progressive steatosis expansion from PC to PP regions during disease progression, paralleled by escalating fibrosis and inflammation. These results suggested that the spatial location of steatosis is highly correlated with MASH severity. Notably, $CD74^+$ LAMs and fibrotic signatures colocalize in the PP zone, mirroring pan-acinar steatosis patterns linked to ballooning and advanced fibrosis in human MASH.[49] These findings position the PP zone as a spatial epicenter for MASH pathogenesis, where metabolic stress and immune activation converge. Surprisingly, CellPhoneDB analysis identified a strong interaction between CD74 and MIF in *Thrsp*-high regions, implicating that the MIF/CD74 signaling pathway, previously linked to inflammatory diseases, was involved in MASH pathology.[50] Additionally, mIHC confirmed spatial overlap among THRSP, CD74, and fibrosis-related markers in the PP zone, highlighting a crucial crosstalk that explained how THRSP drove MASH progression.

Considering the distinct spatial locations of THRSP and $CD74^+$ LAMs, we hypothesized that mediators mediated this cell communication. Insulin resistance promotes hepatic DNL and increases FFA flux to the liver, particularly SFFA like PA, which promotes inflammation.[51] Besides, *Thrsp*-OE elevated hepatic lipogenesis, while *Thrsp* knockdown improved the liver steatosis in *db/db* mice.[28] Consistently, our data established THRSP as a key insulin-responsive regulator of hepatic DNL, driving FASN-mediated PA accumulation. Here, integrating multi-omics (ST, snRNA-seq, lipidomics) with functional assays (flow cytometry, mIHC), we demonstrated that THRSP drove hepatic PA accumulation and recruited monocyte-derived $CD74^+$ LAMs to the hepatic PP zone in MASH. Co-culture experiments confirmed that PA-induced MIF secretion from both hepatocytes and macrophages was the key mediator between THRSP expression and $CD74^+$ LAMs recruitment. Notably, our study uncovers a novel THRSP-mediated FFA synthesis mechanism, wherein THRSP stabilizes FASN by blocking its TRIM21-dependent ubiquitination and degradation.[52,53] These results underscored the role of THRSP in stabilizing FASN, driving increased FFA synthesis in MASH livers.

Notably, the THRSP-targeting compound C6 improves MASH pathology, highlighting its therapeutic potential for clinical translation. Additionally, THRSP coordinates hepatic metabolic-immune crosstalk via the PA–MIF–CD74 axis, where hepatocyte-derived PA motivates MIF secretion to recruit $CD74^+$ LAMs to the PP zone. This spatially restricted mechanism explains the spatial progression of MASH pathology and offers new targets for precision intervention in MASH. While our diet-induced MASH model recapitulates key human transcriptomic signatures, direct validation of the THRSP–$CD74^+$ LAMs axis in human livers remains needed.

DATA AVAILABILITY STATEMENT

The accession number for the spatial transcriptomics sequencing data reported in this paper is GEO: GSE293203.

AUTHOR CONTRIBUTIONS

Xu Xu designed the study, performed most experiments, analyzed data, and wrote the manuscript; Huagen Li, Hai Lin, and Qichao Li performed data analysis of spatial transcriptomics; Yuenan Liu, Weijun Huang, Jundong Yang, Niannian Li, Zhenfei Gao, Shengming Wang, Hangdong Shen, Wenjun Xue, and Haolin Yuan participated in animal experiments; Wei Wang provided human liver samples; Feng Liu and Junli Liu analyzed the data and revised the manuscript. Jianwei Shuai and Shankai Yin supervised the work, analyzed the results, and provided administrative support.

ACKNOWLEDGMENTS

We thank Professor Xu Shen for offering us RAW264.7 cells. We also thank Professors Qiurong Ding, Yongxu Zhao, and Yan Lu for offering us valuable suggestions on the manuscript.

FUNDING INFORMATION

This work was supported by STI2030-Major Projects 2021ZD0201900; National Natural Science Foundation of China (82300962, 81971240); China Postdoctoral Science Foundation under Grant Number 2022M722128; Shanghai Top Priority Research Center—Category B Project (2023ZZ02008); National Natural Science Foundation of China under Grants 12090052 and U24A2014; Shanghai Municipal Commission of Science and Technology (Grant No.18DZ2260200) and Interdisciplinary Program of Shanghai Jiao Tong University (YG2023 LC11).

CONFLICTS OF INTEREST

The authors have no conflicts to report.

ORCID

Xu Xu https://orcid.org/0000–0002–5854–6124

REFERENCES

1. Corey KE, Memel ZN. Bariatric surgery as a strategy for improving outcomes in nonalcoholic steatohepatitis. JAMA. 2021;326:2015–7.
2. Nie Q, Luo X, Wang K, Ding Y, Jia S, Zhao Q, et al. Gut symbionts alleviate MASH through a secondary bile acid biosynthetic pathway. Cell. 2024;187:1–18.
3. Eslam M, Newsome PN, Sarin SK, Anstee QM, Targher G, Romero-Gomez M, et al. A new definition for metabolic dysfunction-associated fatty liver disease: An international expert consensus statement. J Hepatol. 2020;73:202–9.
4. Loomba R, Friedman SL, Shulman GI. Mechanisms and disease consequences of nonalcoholic fatty liver disease. Cell. 2021;184:2537–64.
5. Friedman SL, Neuschwander-Tetri BA, Rinella M, Sanyal AJ. Mechanisms of NAFLD development and therapeutic strategies. Nat Med. 2018;24:908–22.
6. FDA approves first MASH drug. J Nat Biotechnol. 2024;42:540.
7. Halpern KB, Shenhav R, Matcovitch-Natan O, Tóth B, Lemze D, Golan M, et al. Single-cell spatial reconstruction reveals global division of labour in the mammalian liver. Nature. 2017;542:352–6.
8. Batchuluun B, Pinkosky SL, Steinberg GR. Lipogenesis inhibitors: Therapeutic opportunities and challenges. Nat Rev Drug Discov. 2022;21:283–305.
9. Gu L, Zhu Y, Watari K, Lee M, Liu J, Perez S, et al. Fructose-1,6-bisphosphatase is a nonenzymatic safety valve that curtails AKT activation to prevent insulin hyperresponsiveness. Cell Metab. 2023;35:1009–21.e9.
10. Porstmann T, Santos CR, Griffiths B, Cully M, Wu M, Leevers S, et al. SREBP activity is regulated by mTORC1 and contributes to Akt-dependent cell growth. Cell Metab. 2008;8:224–36.
11. Smith GI, Shankaran M, Yoshino M, Schweitzer GG, Chondronikola M, Beals JW, et al. Insulin resistance drives hepatic de novo lipogenesis in nonalcoholic fatty liver disease. J Clin Invest. 2020;130:1453–60.
12. Huby T, Gautier EL. Immune cell-mediated features of nonalcoholic steatohepatitis. Nat Rev Immunol. 2021;22:429–43.
13. Barreyro FJ, Kobayashi S, Bronk SF, Werneburg NW, Malhi H, Gores GJ. Transcriptional regulation of Bim by FoxO3A mediates hepatocyte lipoapoptosis. J Biol Chem. 2007;282:27141–54.
14. Masuoka HC, Mott J, Bronk SF, Werneburg NW, Akazawa Y, Kaufmann SH, et al. Mcl-1 Degradation during hepatocyte lipoapoptosis. J Biol Chem. 2009;284:30039–48.
15. Schuppan D, Surabattula R, Wang XY. Determinants of fibrosis progression and regression in NASH. J Hepatol. 2018;68:238–50.
16. Feldstein AE, Canbay A, Angulo P, Taniai M, Burgart LJ, Lindor KD, et al. Hepatocyte apoptosis and Fas expression are prominent features of human nonalcoholic steatohepatitis. Gastroenterology. 2003;125:437–43.
17. Lefere S, Puengel T, Hundertmark J, Penners C, Frank AK, Guillot A, et al. Differential effects of selective- and pan-PPAR agonists on experimental steatohepatitis and hepatic macrophages. J Hepatol. 2020;73:757–70.
18. Xiong X, Kuang H, Ansari S, Liu T, Gong J, Wang S, et al. Landscape of intercellular crosstalk in healthy and NASH liver revealed by single-cell secretome gene analysis. Mol Cell. 2019;75:644–660.e5.
19. Jaitin DA, Adlung L, Thaiss CA, Weiner A, Li B, Descamps H, et al. Lipid-associated macrophages control metabolic homeostasis in a Trem2-dependent manner. Cell. 2019;178:686–698.e14.
20. Zhou L, Qiu X, Meng Z, Liu T, Chen Z, Zhang P, et al. Hepatic danger signaling triggers TREM2(+) macrophage induction and drives steatohepatitis via MS4A7-dependent inflammasome activation. Sci Transl Med. 2024;16:eadk1866.
21. Remmerie A, Martens L, Thoné T, Castoldi A, Seurinck R, Pavie B, et al. Osteopontin expression identifies a subset of recruited macrophages distinct from Kupffer cells in the fatty liver. Immunity. 2020;53:641–657.e14.
22. Zheng S, Ren X, Han T, Chen Y, Qiu H, Liu W, et al. Fenofibrate attenuates fatty acid-induced islet β-cell dysfunction and apoptosis via inhibiting the NF-κB/MIF dependent inflammatory pathway. Metabolism. 2017;77:23–38.
23. Marin V, Poulsen K, Odena G, McMullen MR, Altamirano J, Sancho-Bru P, et al. Hepatocyte-derived macrophage migration inhibitory factor mediates alcohol-induced liver injury in mice and patients. J Hepatol. 2017;67:1018–25.
24. Bernhagen J, Krohn R, Lue H, Gregory JL, Zernecke A, Koenen RR, et al. MIF is a noncognate ligand of CXC chemokine receptors in inflammatory and atherogenic cell recruitment. Nat Med. 2007;13:587–96.
25. Poulsen KL, Fan XD, Kibler CD, Huang E, Wu X, McMullen MR, et al. Role of MIF in coordinated expression of hepatic chemokines in patients with alcohol-associated hepatitis. JCI Insight. 2021;6:e141420.
26. Aipoalani DL, O'Callaghan BL, Mashek DG, Mariash CN, Towle HC. Overlapping roles of the glucose-responsive genes, S14 and S14R, in hepatic lipogenesis. Endocrinology. 2010;151:2071–7.
27. Sinha RA, Singh BK, Yen PM. Direct effects of thyroid hormones on hepatic lipid metabolism. Nat Rev Endocrinol. 2018;14:259–69.
28. Wu J, Wang C, Li S, Li S, Wang W, Li J, et al. Thyroid hormone-responsive SPOT 14 homolog promotes hepatic lipogenesis, and its expression is regulated by liver X receptor alpha through a sterol regulatory element-binding protein 1c-dependent mechanism in mice. Hepatology. 2013;58:617–28.
29. Ma L, Tsatsos NG, Towle HC. Direct role of ChREBP.Mlx in regulating hepatic glucose-responsive genes. J Biol Chem. 2005;280:12019–27.
30. Moreau A, Téruel C, Beylot M, Albalea V, Tamasi V, Umbdenstock T, et al. A novel pregnane X receptor and S14-mediated lipogenic pathway in human hepatocyte. Hepatology. 2009;49:2068–79.

31. Asgharpour A, Cazanave SC, Pacana T, Seneshaw M, Vincent R, Banini BA, et al. A diet-induced animal model of non-alcoholic fatty liver disease and hepatocellular cancer. J Hepatol. 2016;65:579–88.
32. Wang L, Zhang X, Lin Z-B, Yang PJ, Xu H, Duan JL, et al. Tripartite motif 16 ameliorates nonalcoholic steatohepatitis by promoting the degradation of phospho-TAK1. Cell Metab. 2021; 33:1372–388.e7.
33. Vacca M, Kamzolas I, Harder LM, Oakley F, Trautwein C, Hatting M, et al. An unbiased ranking of murine dietary models based on their proximity to human metabolic dysfunction-associated steatotic liver disease (MASLD). Nat Metab. 2024;6:1178–96.
34. Guilliams M, Bonnardel J, Haest B, Vanderborght B, Wagner C, Remmerie A, et al. Spatial proteogenomics reveals distinct and evolutionarily conserved hepatic macrophage niches. Cell. 2022; 185:379–396.e38.
35. Gao S, Shi Q, Zhang Y, Liang G, Kang Z, Huang B, et al. Identification of HSC/MPP expansion units in fetal liver by single-cell spatiotemporal transcriptomics. Cell Res. 2021;32:38–53.
36. Ji AL, Rubin AJ, Thrane K, Jiang S, Reynolds DL, Meyers RM, et al. Multimodal analysis of composition and spatial architecture in human squamous cell carcinoma. Cell. 2020;182:497–514.e22.
37. Kleshchevnikov V, Shmatko A, Dann E, Aivazidis A, King HW, Li T, et al. Cell2location maps fine-grained cell types in spatial transcriptomics. Nat Biotechnol. 2022;40:661–71.
38. Seidman JS, Troutman TD, Sakai M, Gola A, Spann NJ, Bennett H, et al. Niche-specific reprogramming of epigenetic landscapes drives myeloid cell diversity in nonalcoholic steatohepatitis. Immunity. 2020;52:1057–74.e7.
39. Vento-Tormo R, Efremova M, Botting RA, Turco MY, Vento-Tormo M, Meyer KB, et al. Single-cell reconstruction of the early maternal–fetal interface in humans. Nature. 2018;563:347–53.
40. Savitski MM, Reinhard FBM, Franken H, Werner T, Savitski MF, Eberhard D, et al. Tracking cancer drugs in living cells by thermal profiling of the proteome. Science. 2014;346:1255784.
41. Li Q, Zhang L, Yang Q, Li M, Pan X, Xu J, et al. Thymidine kinase 1 drives hepatocellular carcinoma in enzyme-dependent and -independent manners. Cell Metab. 2023;35:912–927.e7.
42. Lu X, Kong X, Wu H, Hao J, Li S, Gu Z, et al. UBE2M-mediated neddylation of TRIM21 regulates obesity-induced inflammation and metabolic disorders. Cell Metab. 2023;35:1390–1405.e8.
43. Lan T, Hu Y, Hu F, Li H, Chen Y, Zhang J, et al. Hepatocyte glutathione S-transferase mu 2 prevents non-alcoholic steatohepatitis by suppressing ASK1 signaling. J Hepatol. 2022;76: 407–19.
44. Peng JY, Cai DK, Zeng RL, Zhang CY, Li GC, Chen SF, et al. Upregulation of superenhancer-driven LncRNA FASRL by USF1 promotes de novo fatty acid biosynthesis to exacerbate hepatocellular carcinoma. Adv Sci. 2022;10:e2204711.
45. Schuster S, Cabrera D, Arrese M, Feldstein AE. Triggering and resolution of inflammation in NASH. Nat Rev Gastroenterol Hepatol. 2018;15:349–64.
46. Ibrahim SH, Hirsova P, Gores GJ. Non-alcoholic steatohepatitis pathogenesis: Sublethal hepatocyte injury as a driver of liver inflammation. Gut. 2018;67:963–72.
47. Zhang F, Hu Z, Li G, Huo S, Ma F, Cui A, et al. Hepatic CREBZF couples insulin to lipogenesis by inhibiting insig activity and contributes to hepatic steatosis in diet-induced insulin-resistant mice. Hepatology. 2018;68:1361–75.
48. Lin P, Yan X, Jing S, Wu Y, Shan Y, Guo W, et al. Single-cell and spatially resolved transcriptomics for liver biology. Hepatology. 2024;80:698–720.
49. Chalasani N, Wilson L, Kleiner DE, Cummings OW, Brunt EM, Ünalp A. Relationship of steatosis grade and zonal location to histological features of steatohepatitis in adult patients with non-alcoholic fatty liver disease. J Hepatol. 2008;48:829–34.
50. Shi X, Leng L, Wang T, Wang W, Du X, Li J, et al. CD44 is the signaling component of the macrophage migration inhibitory factor-CD74 receptor complex. Immunity. 2006;25:595–606.
51. Marra F, Svegliati-Baroni G. Lipotoxicity and the gut–liver axis in NASH pathogenesis. J Hepatol. 2018;68:280–95.
52. Lin H-P, Cheng Z-L, He R-Y, Song L, Tian MX, Zhou LS, et al. Destabilization of fatty acid synthase by acetylation inhibits de novo lipogenesis and tumor cell growth. Cancer Res. 2016;76: 6924–36.
53. Xu S, Wu X, Wang S, Xu M, Fang T, Ma X, et al. TRIM56 protects against nonalcoholic fatty liver disease by promoting the degradation of fatty acid synthase. J Clin Invest. 2024;134:e166149.

How to cite this article: Xu X, Li H, Lin H, Li Q, Liu Y, Huang W, et al. MIF-mediated crosstalk between THRSP^{+} hepatocytes and CD74^{+} lipid-associated macrophages in hepatic periportal zone drives MASH. Hepatology. 2025;■■:■■–■■. https://doi.org/10.1097/HEP.0000000000001429